CHALMERS
UNIVERSITY OF TECHNOLOGY

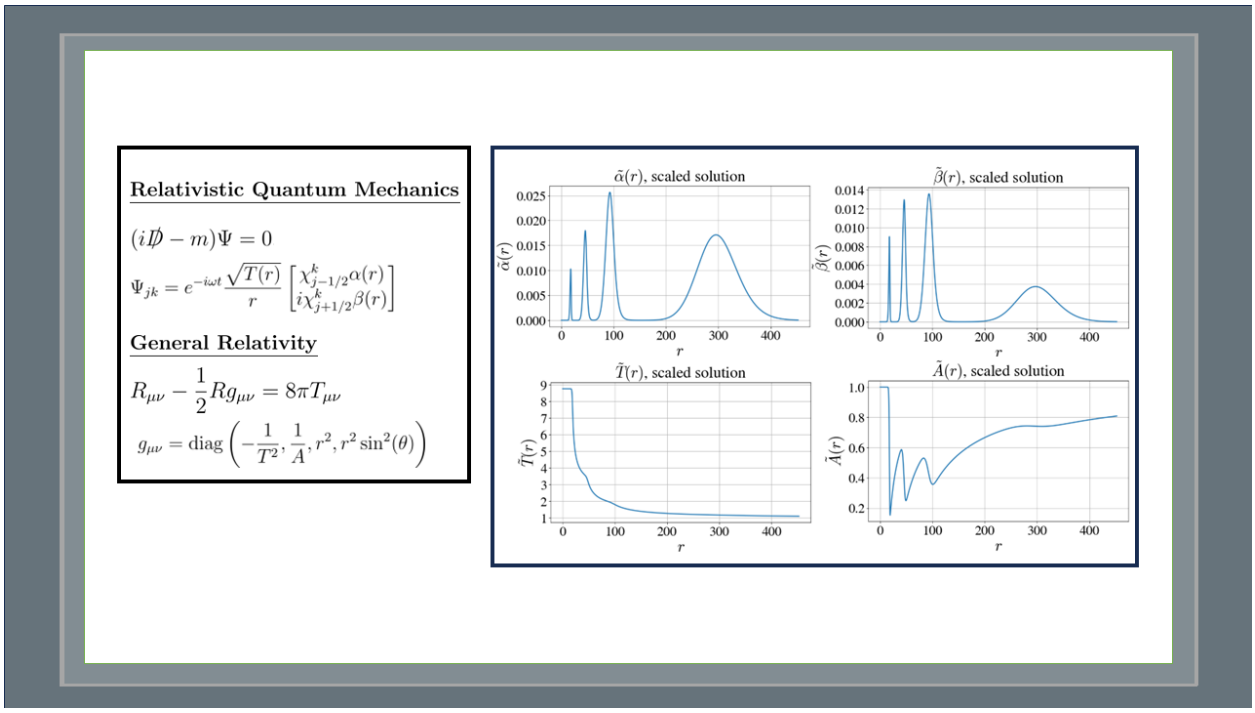

Static solutions of the Einstein-Dirac system for an increasing number of particles behave as solutions of the Einstein-Vlasov system

A study of the transition to classical behaviour for a quantum system

Master's thesis in Engineering Mathematics and Computational Science

JOAKIM BLOMQVIST

DEPARTMENT OF MATHEMATICS
CHALMERS UNIVERSITY OF TECHNOLOGY
Gothenburg, Sweden 2023
www.chalmers.se

Master's thesis 2023

Static solutions of the Einstein-Dirac system for an increasing number of particles behave as solutions of the Einstein-Vlasov system

A Study of the transition to classical behaviour of a quantum system and comparing properties of a classical and quantum matter distribution

JOAKIM BLOMQVIST

CHALMERS
UNIVERSITY OF TECHNOLOGY

Department of Mathematics
Division of Analysis and Probability Theory
Mathematical Physics
Chalmers University of Technology
Gothenburg, Sweden 2023

Static solutions of the Einstein-Dirac system for an increasing number of particles behave as solutions of the Einstein-Vlasov system.
A Study of the transition to classical behaviour of a quantum system and comparing properties of a classical and quantum matter distribution.
JOAKIM BLOMQVIST

Supervisor: Håkan Andréasson, Department of Mathematics
Examiner: Håkan Andréasson, Department of Mathematics

Master's Thesis 2023
Department of Mathematics
Division of analysis and probability theory
Mathematical physics
Chalmers University of Technology
SE-412 96 Gothenburg
Telephone +46 31 772 1000

Cover: An illustration of the involved equations, and a set of solutions to the Einstein-Dirac equations

Typeset in LaTeX
Printed by Chalmers Reproservice
Gothenburg, Sweden 2023

Static solutions of the Einstein-Dirac system for an increasing number of particles behave as solutions of the Einstein-Vlasov system.
A Study of the transition to classical behaviour of a quantum system and comparing properties of a classical and quantum matter distribution.
JOAKIM BLOMQVIST
Department of Mathematics
Chalmers University of Technology

Abstract

In this thesis we will study static solutions to the spherically symmetric Einstein-Dirac system. This system couples Einstein's theory of general relativity to Dirac's relativistic description of quantum mechanics. The goal was to study the transition from a quantum mechanical description to a classical description by comparing properties of the solutions to the Einstein-Dirac system to solutions of the Einstein-Vlasov system as the number of particles of the former system increases. In 1999 Finster et al. [10] found for the first-time static solutions to the Einstein-Dirac system in the case of two fermions with opposite spins. Recently this study has been extended to a larger number of particles by Leith et al [14]. In particular, they construct highly relativistic solutions. The structure of the solutions is strikingly similar to the structure of highly relativistic solutions of the Einstein-Vlasov system. In both cases multi-peak solutions are obtained, and moreover, the maximum compactness of the solutions is very similar. The compactness is measured by the quantity m/r, where m is the mass and r the areal radius, and in both cases the maximum value appears to be 4/9. Furthermore, in quantum mechanics the pressure may be negative whereas classically it is non-negative. We find that already for 16 particles the pressure is non-negative and thus behaves classically. In order to compare the solutions, I need to construct solutions numerically to the Einstein-Dirac system in the case of a large number of particles. This requires a delicate procedure with significant numerical precision when the number of particles in the system grows.

Keywords: General relativity, relativistic quantum mechanics, phenomenological matter model, field theoretic matter model.

Acknowledgements

Being able to work on a project in this subject area, has been personal goal of mine and served as my main motivation for studying physics at Chalmers. Hence, I must express sincere gratitude towards my supervisor Håkan, for both introducing me to this project and for our many discussions about mathematics, physics and life in general. Our discussions were very helpful, especially during the initial stages, when I had great numerical difficulties. On a personal note, I must also express a deep gratitude towards my family and also Pernilla, I cannot thank you enough for your support while working on this project. Finally, I must also thank Oskar for giving me detailed feedback on some sections of this report and my many friends I have made during my time at Chalmers and GU.

Joakim Blomqvist, Gothenburg, November 2023

Contents

List of Figures

1

Introduction

This thesis work investigates properties of two matter distributions emergent from two seemingly very different relativistic matter models. The models are in order of emphasis, the Einstein-Dirac system, and the Einstein-Vlasov system. Physically, both models are phenomenologically very different, the first named system involves matter described by a quantum wavefunction, making the matter model stochastic, while the latter is a matter model describing the distribution of deterministic classical matter. Microscopically all matter is modelled using wavefunctions, but given enough particles, there is a limit where matter is purely deterministic and thus classical in nature. This implies that there is a transition occurring or simply that the random nature of individual particles, akin to the central limit theorem, averages out to deterministic behavior. This is a philosophical question many physicists have grappled with during the emergence of quantum mechanics, in particular, Albert Einstein famously disliked the idea that the fundamental building blocks of the universe are not deterministic; one of his many famous quotes are "God does not play dice with the universe".

Putting that philosophical question aside, quantum theory despite this, has proven itself by experiment to be a theory with great predictive power and accuracy. One important branch of quantum theory is Dirac's relativistic description of quantum mechanics, which gave birth to the field of quantum field theory, and predicted with great accuracy, the fine structure splitting of quantum states caused by the spin of electrons. Another great accomplishment of the theory is also the at first, paradoxical prediction of anti-matter, which is due to the mathematical formulation of the governing equation. As was discussed previously there should exist a transition of quantum behavior towards classical behavior, and this is the main motivation for studying both the Einstein-Vlasov and the Einstein-Dirac system.

On the surface, the main similarity between both systems, is that gravitational interaction is described by Einstein's field equations. The underlying theory behind the equations are flexible enough to model gravitational effects in terms of space time curvature, for many kinds of matter behavior. Similarly, to quantum mechanics, Einstein's general theory of relativity has also proven itself to be an accurate model based on several experimental observations, most recently is the detection of gravitational waves. Thus, studying a model constructed by coupling both theories must yield interesting results. However, it is worth remarking that in modern physics, physicists are searching for a quantized theory of gravity, as general relativity breaks down at small scales. Hence, a quantum model affected by gravitational

effects described Einstein's field equations, is physically an approximation.

The Einstein-Dirac system was at first studied by Felix Finster, Joel Smoller and Shing-Tung Yau in their paper [10]. In said paper they both derived the system for two fermions in a spherically symmetric static spacetime and generated numerical solutions for the resulting differential equations. These solutions had two key properties, and those are in no particular order, a non-singular center and an asymptotically flat metric tensor. The final property implies that the resulting metric tensor from the Einstein-Dirac system converges to the Minkowski tensor, while also intersecting with the Schwarzschild metric. More recently a series of papers have been published by a group from the University of St Andrews, see for example [14] & [5]. In these papers they considered a more general version of the Einstein-Dirac system, to be more specific, they studied a system with an arbitrary number of fermions. These solutions with a certain level of central redshift, appeared to be very similar to matter distributions produced by the Einstein-Vlasov system. This apparent similarity acted as the main motivation for pursing this project. Since the Einstein-Vlasov system is constructed by a classical matter distribution, also known as a Boltzmann distribution. Based on these similarities and the phenomena of a quantum system acting more classically for an increasing number of particles, there seemed to be an interesting connection between a quantum system and classical system, which was previously unknown territory. At a first glance these models appear to form an interesting pairing for studying the transition from quantum to classical matter behavior. Hence, the aim of thesis is to explores the Einstein-Dirac and Einstein-Vlasov systems, to shed light on this transition from quantum to classical matter behavior and uncover the connections between these seemingly distinct systems.

2

Mathematical preliminaries

This chapter will provide some necessary mathematical background for the interested reader and give them a better foundation to grasp the results and analysis performed in this work. Note that the mathematical foundations for general relativity are both complex and extensive and is built on different branches of mathematics such as differential geometry, differential forms, topology, and group theory to name a few.

2.1 The Einstein summation convention

The equations of general relativity are constructed using tensors V^i_j, where the elements of a tensor are referenced by indices $i, j \in \mathbb{N}$. The location of the indices is important, since they refer to different vector spaces; the upper indices V^i are known as contravariant tensor components while lower indices, V_i are known as covariant components. The meaning of these will be made more precise shortly. The Einstein summation convention is a shorthand notation for sums over tensor components. To be more precise, it is a convention that implicitly defines a summation over upper and lower indices if they possess matching symbols,

$$V^i V_i = \sum_{i \in \mathcal{I}} V^i V_i, \tag{2.1}$$

where $\mathcal{I}$ denotes a general index set. It is nonetheless a popular convention, since it simplifies equation by removing any summation symbols, which would quickly become cumbersome, for Einstein's field equations. In general relativity the letters used to denote indices are sometimes used to identify the basis for which the component of the tensor emerges from. According to convention, Greek letters signify elements of a Minkowski or Lorentzian space, while Latin letters are used either to denote components of a Riemannian space or a general undefined space, where the index is not identified with a basis. Given the nature of this work, all relevant equations are written in a Lorentzian spacetime, and thus all tensor components in the theory section and beyond, will be referenced with Greek letters.

2.2 Definition of a spacetime

In opposition to the conventional theory for partial differential equations, the domain is not static, more concretely, the geometry of the region is coupled to matter behavior. This key idea distinguishes the classical theory of gravity constructed by Isaac Newton and general relativity founded by Albert Einstein. The region of

interest in this case is known as a spacetime, which is constructed by a manifold $\mathcal{M}$ and an object which can be applied to study the local geometry about a point in $\mathcal{M}$, a metric g. Together they yield a spacetime description $(\mathcal{M}, g)$. The definition of the metric will be introduced in its own subsection, and we will therefor concentrate on the definition of a manifold for the remainder of this section.

A manifold is a set made up of smaller constituents, which are open subsets that can smoothly be joined together. General relativity employs real manifolds, and we will define them using the definition provided by Wald.

Definition 2.2.1 (Smooth real manifolds [26]) *A n dimensional C^∞ real manifold $\mathcal{M}$, is a set together with a collection of subsets $\{O_\alpha\}$ satisfying.*

- *Each $p \in \mathcal{M}$ lies in at least one subset O_α, i.e. subsets $\{O_\alpha\}$ cover $\mathcal{M}$.*
- *For each α there is a bijective map $\psi_\alpha : O_\alpha \to U_\alpha$, where U_α is an open subset of $\mathbb{R}^n$.*
- *If any two sets O_α, O_β overlap, then $O_\alpha \cap O_\beta \neq \emptyset$, we can consider a map $\psi_\beta \circ \psi_\alpha^{-1}$ which takes points in $\psi_\alpha[O_\alpha \cap O_\beta] \subset U_\alpha \subset \mathbb{R}^n$ to points in $\psi_\beta[O_\alpha \cap O_\beta] \subset U_\beta \subset \mathbb{R}^n$. We require that U_α, U_β are open and that this map is C^∞.*

The maps ψ, are both known as charts or coordinate system maps, the latter terminology will henceforth be used.

A point p on a manifold $\mathcal{M}$, is represented using an upper index p^i, where the index $i \in \{0, 1, 2, 3\}$, for a (1+3) dimensional manifold. Conventionally, the first index p^0, specifies the time coordinate of a point while the remaining indices specifies a spatial coordinate, defined by a coordinate system. In the case of a spherical coordinate system, the remaining indices $\{1, 2, 3\}$ is associated with the radial basis-$e_1 = e_r$, and the angular basis functions $e_2 = e_\theta$ and $e_3 = e_\varphi$, which are defined by the regular Cartesian basis $\{\hat{x}, \hat{y}, \hat{z}\}$ as follows:

$$
\begin{aligned}
e_r &= \sin\theta\cos\varphi\,\hat{x} + \sin\theta\sin\varphi\,\hat{y} + \cos\theta\,\hat{z},\\
e_\theta &= \cos\theta\cos\varphi\,\hat{x} + \cos\theta\sin\varphi\,\hat{y} - \sin\theta\,\hat{z},\\
e_\varphi &= -\sin\varphi\,\hat{x} + \cos\varphi\,\hat{y}.
\end{aligned}
$$

2.3 Dual spaces and tangent spaces

Let V be a vector space and let V^* denote a set of linear maps $L : V \to \mathbb{R}$. Since the family of maps L, are linear, we immediately recover a vector space structure for V^* as-well.

Indeed, let $u, v \in V$, then $L(u + v) = L(u) + L(v)$;
furthermore, let $\alpha, \beta \in \mathbb{C}$, then $L(\alpha v + \beta v) = L(\alpha u) + L(\beta v) = \alpha L(u) + \beta L(v)$.

The set of linear maps can therefore be shown to obey all axioms for a vector space. This new vector space V^* is known as the *dual space* to V. As a matter of fact, the natural norm for this space is the operator norm,

$$\|L\| = \sup_{\|x\|=1} \|L(x)\|.$$

Elements of a dual space are known as dual vectors. In general relativity V is defined locally on a manifold, and in particular in this work $\mathcal{M} \subseteq \mathbb{R}^{(1,3)}$, where the notation $(1,3)$ implies an inherent distinction between one time dimension and three spatial dimensions. This distinction will be made more mathematically precise in the section about the metric tensor. The dual space for the vector space in general relativity is a linear functional also defined by the metric tensor; the linear functional is in this case a special inner product.

Vector spaces employed in general relativity are known as tangent spaces. All tensors or tensor fields are defined locally on a point's tangent space, $p \in \mathcal{M}$. These spaces were introduced to give rise to a vector space structure on a manifold, since manifolds does not naturally exhibit the necessary properties. To illustrate this fact, consider a manifold defined by

$$\mathcal{M} := \left\{ x \in \mathbb{R}^3 : \ \|x\|^2 = x_1^2 + x_2^2 + x_3^2 = c^2, \text{ where } c \in \mathbb{R} \right\}.$$

Take two arbitrary elements $u, v \in \mathcal{M}$, and consider the image of an arbitrary linear combination of these elements,

$$f(u, v; a, b) := au + bv, \quad a, b \in \mathbb{R}.$$

To prove that f is not in general an element of $\mathcal{M}$, consider the following argument,

$$\begin{aligned} &f \in \mathcal{M} \Leftrightarrow \|f\| = c, \\ &\|f\| = \|au + bv\| \leq |a|\|u\| + |b|\|v\| = c(|a| + |b|) \neq c \ \ \forall\, a, b \in \mathbb{R}. \end{aligned}$$

By the analysis above, f is not in general a map into $\mathcal{M}$, and hence $\mathcal{M}$ is not a proper vector space. We can therefor assert that points on manifolds does not inherently have properties of a vector space, which necessitates the introduction of tangent spaces. Opposed to vector spaces in the theory of differential equations, tangent spaces are defined locally for all points on a manifold.

Definition 2.3.1 (Tangent vectors and tangent spaces [18][26]) *Let $\mathcal{M}$ be a smooth differentiable manifold, and $\mathfrak{F}(\mathcal{M})$ be the set of smooth functions (C^∞) on $\mathcal{M}$. Then a tangent vector v is a map $v : \mathfrak{F}(\mathcal{M}) \to \mathbb{R}$, with the following properties:*

$$\begin{aligned} &\textit{(1):} \quad v(af + bg) = av(f) + bv(g), \ \ \forall a, b \in \mathbb{R} \textit{ and } \forall f, g \in \mathfrak{F}(\mathcal{M}); \\ &\textit{(2):} \quad v(fg) = v(f)g + v(g)f, \ \ \forall f, g \in \mathfrak{F}(\mathcal{M}). \end{aligned}$$

A tangent space centred at p on $\mathcal{M}$, is then the set of all such tangent vectors and is denoted by $T_p\mathcal{M}$. The basis for $T_p\mathcal{M}$ is given by differential operators, that are locally mapping functions $f \in \mathfrak{F}(\mathcal{M})$ to real numbers, $D_{i|p} : \mathfrak{F}(\mathcal{M}) \to \mathbb{R}$,

$$D_{i|p} := \frac{\partial}{\partial x^i}\Big|_p, \quad \forall f \in C^1(\mathcal{M}) : \ D_{i|p}(f) = \frac{\partial f}{\partial x^i}(p). \tag{2.2}$$

Finally, let $x^i = (x^0, \dots, x^n)$ *when* $n \in \mathbb{N}$*, be a coordinate system with a corresponding basis* $\hat{x}^i$*. Then using the basis* $D_{i|p}$*, we can represent all elements of* $T_p\mathcal{M}$ *by the possible linear combinations of the basis and tangent vectors* v

$$\forall v \in T_p\mathcal{M},\ v = \sum_{i=0}^{n} v(x^i) \frac{\partial}{\partial x^i}\Big|_p, \quad v : \mathfrak{F}(\mathcal{M}) \to \mathbb{R}.$$

Tangent spaces, employs directional derivative operators to yield locally defined vectorspaces. Indeed, since differential operators are linear, all relevant properties follow as a result. Furthermore, due to the restriction of differentiable manifolds, the class $\mathfrak{F}(\mathcal{M})$ will ensure that they are bounded.

2.4 Tensor formalism

In this section we will discuss some necessary theory used to rigorously define tensors, to give some background to Einstein's field equations. All the provided equations and information about the theoretical background of general relativity, unless explicitly stated otherwise, are based on material found in either [26] or [27]. Both books are classics and provides a solid theoretical foundation for the subject.

2.4.1 Tensor definitions

Tensor equations are central to general formulations of physical laws, since the underlying formalism, yields equations whose corresponding physical laws are invariant to the coordinates in which the theory is formulated. In physics the philosophy, "if it looks like a duck, acts like a duck and quacks like a duck, then it is a duck" is often applied to define tensor objects. More concretely, through this lens, they can be viewed as objects whose components transform in a special way. The transformation laws are different for contravariant- and covariant components. These components are elements of tangent spaces and their dual spaces, respectively. To discuss and introduce these laws, we will introduce two sets of coordinates x^i and ξ^j, where the first is informally known as the "un-primed coordinates" and the latter are known as the "primed coordinates". More formally, to define the first transformation law, we require two sets of coordinate systems generated by two sets of basis elements.

Definition 2.4.1 (Prime and un-primed coordinate systems) *Let* x^a *denote a set of elements emergent from the basis* $\{v^a\}_{a\in\mathcal{I}}$ *where* $\mathcal{I} \subset \mathbb{N}$*. The basis elements* v^a*, naturally, span the vector space* V*. Correspondingly, let* ξ^a *denote a set of elements emergent from the basis* $\left\{(v')^b\right\}_{b\in\mathcal{J}}$ *where* $\mathcal{J} \subset \mathbb{N}$*, which spans another vector space* V'*.*
Given this definition, a tensor transformation, is a map $u \mapsto u'$, that maps elements from a proper vector space $u \in V$, to another vector space $u' \in V'$, described by two different coordinate systems x^a and ξ^a, according to the following transformation law,

$$(u')^a = \frac{\partial \xi^a}{\partial x^p} u^p. \tag{2.3}$$

Similarly, the corresponding transformation law for a dual space element $u_a \mapsto u'_a$ is defined as

$$(u')_a = \frac{\partial x^p}{\partial \xi^a} u_p. \tag{2.4}$$

Both transformation laws define maps for tensors of rank one, between vector spaces or dual spaces. The transformation laws generalize to higher rank tensor with the tensor product, that is $T^{ab} = U^a \otimes V^b$, and hence, a transformation of a degree two or higher tensor, is defined by component wise, applying the appropriate rank one transformation law:

$$\begin{aligned}(T')^{ab} = (U')^a \otimes (V')^b &= \left(\frac{\partial \xi^a}{\partial x^p} U^p\right) \otimes \left(\frac{\partial \xi^b}{\partial x^q} V^q\right) \\ &= \frac{\partial \xi^a}{\partial x^p}\frac{\partial \xi^b}{\partial x^q} U^p \otimes V^q = \frac{\partial \xi^a}{\partial x^p}\frac{\partial \xi^b}{\partial x^q} T^{pq},\end{aligned}$$

$$\begin{aligned}(T')_{ab} = (U')_a \otimes (V')_b &= \left(\frac{\partial x^p}{\partial \xi^a} U_p\right) \otimes \left(\frac{\partial x^q}{\partial \xi^b} V_q\right) \\ &= \frac{\partial x^p}{\partial \xi^a}\frac{\partial x^q}{\partial \xi^b} U_p \otimes V_q = \frac{\partial x^p}{\partial \xi^a}\frac{\partial x^q}{\partial \xi^b} T_{pq}.\end{aligned}$$

Higher order transformation laws can be derived using the same procedure by writing $T^{a_1 a_2 \dots a_n} = T^{a_1} \otimes T^{a_2} \dots T^{a_{n-1}} \otimes T^{a_n}$, where n, $a_n \in \mathbb{N}$. Finally, we will also study an equation, constructed by tensors with mixed indices. To define their transformation behavior, consider a rank two case $T^a_{\ b} = U^a \otimes V_b$, each component in the tensor product transforms using its previously defined transformation map, and hence the tensor transforms according to

$$(T')^a_{\ b} = (U')^a \otimes (V')_b = \frac{\partial \xi^a}{\partial x^p}\frac{\partial x^q}{\partial \xi^b} T^p_{\ q}. \tag{2.5}$$

Transformations of higher ranked mixed index tensors, generalizes precisely as a tensor with only one type of index, using the same tensor product formalism.

This more pragmatic definition is useful in a physical context but must be expanded upon to discuss it more rigorously. To this end let V be a finite dimensional vector space and let V^* denote its dual space. Then a tensor T, of type (k, l) over V is a multilinear map

$$T : \underbrace{V^* \times V^* \times \ldots \times V^*}_{k\text{-times}} \times \underbrace{V \times V \times \ldots \times V}_{l\text{-times}} \to \mathbb{R}, \tag{2.6}$$

using index notation it can be written as $T^{a_0 a_1 \dots a_l}_{b_0 b_1 \dots b_k}$. The multilinearity property also implies that a tensor is an element of a vector space denoted by $\mathscr{I}(k, l)$. There are a few tensor operations, one of them is contraction. Contraction directly operates on the indices of a tensor, and redefines the symbol used for either a covariant or

a contravariant index to gain a matching pair of indices. Consequently, the tensor reduces in order due to the resulting summation:

$$V^{ij}V_{kl} \overset{l=j}{\rightarrow} V^{ij}V_{kj} = \sum_j V^{ij}V_{kj}. \tag{2.7}$$

Circling back to the tensor product discussed earlier, which is also known as an outer product, can be made more precise using this formalism. Take two tensors $U \in \mathscr{I}_U(a,b)$ and $V \in \mathscr{I}_V(c,d)$, where $a,b,c,d \in \mathbb{N}$, then the operation $U \otimes V$, yields a new tensor, $T = U \otimes V$, from the corresponding tensor space $T \in \mathscr{I}_{U\otimes V}(a+c, b+d)$.

2.4.2 The metric tensor

Linear algebra, or elementary vector calculus, studies vectors from an elementary vector space $V = \mathbb{R}^n$, using an inner product $\langle \cdot | \cdot \rangle : V \times V \to \mathbb{R}$,

$$\langle u|v\rangle = \sum_i u_i v_i, \quad u, v \in \mathbb{R}^n. \tag{2.8}$$

In conjunction the vector space and the inner product forms a metric space $(\mathbb{R}^n, d)$, where $d(x,y) = \|x-y\| = \sqrt{\langle x-y|x-y\rangle}$. Using the inner product (2.8), we can define lengths of vectors, and angles between vectors in our vector space V

$$\|x\| = \sqrt{\langle x|x\rangle}, \quad \cos(\theta) = \frac{\langle x|y\rangle}{\|x\|\|y\|}. \tag{2.9}$$

It also follows that these metric spaces, are natural for so-called flat Euclidean or Riemannian geometries, which is the fundamental spaces of classical physics. In general relativity however, the inherent spatial and temporal dimensions are not static, and can be intrinsically curved, which requires more complex mathematical formalism. For all vector fields (or events) in the spacetime manifold $\mathcal{M}$, a corresponding inner product operation g, is known as a *metric* or *metric tensor* [18]

$$g \triangleq \langle \cdot | \cdot \rangle = g_{ab}, \quad a, b \in \mathbb{N}. \tag{2.10}$$

With the metric, an inner product between spacetime vectors $u, v \in \mathcal{M}$ can be written as follows

$$g(u,v) = \langle u|v\rangle = g_{ab}u^a v^b. \tag{2.11}$$

The metric naturally, acts as an isomorphism between the regular vector space and its dual $V \cong V^*$. Hence, elements of the dual space u_a can be accessed or defined by employing the metric,

$$u_a = g(u, \cdot) = g_{ab}u^b. \tag{2.12}$$

Note that the use of repeated upper and lower indices, implicitly defines a summation over them. Also make a note of the fact that the metric tensor yields a weighted version of the regular Euclidean scalar product (2.8). These weights are important, as they will be used to transmit the influence of intrinsically non-flat or non-Riemannian geometry upon lengths of, and angles between vectors. Minkowskian spacetimes, in contrast to Riemannian geometries have a non-definite metric tensor,

since in a Riemannian spacetime $g_{ab} = \delta_{ab}$ where δ is the well-known Kronecker delta tensor, also known as an identity matrix, yields a positive definite norm induced by the inner product $\|u\|^2 = \langle u|u\rangle = g_{ab}u^a u^b$. In Minkowskian spacetime, this definition of a norm is not positive definite any longer, and hence does not obey the properties of a metric, to form a metric space. This fact is caused by a deliberate partitioning of the dimensions of a $\mathbb{R}^n$ space into two distinct categories, where one is the time dimensions and the other are the spatial dimensions. Elements of the metric tensor associated with each set, are distinguished by a relative minus sign; this defines the signature of the metric, and is often denoted by the notation $(-,+,+,+)$ or $\mathbb{R}^{(1,3)}$. The set incurring the negative metric tensor components is arbitrary, and in the previous example, the first dimension x^0 is by convention a time dimension, this implies that $g_{00} < 0$. In physics there is an important distinction between a Minkowski and Lorentzian spacetime, the latter is a more general environment, where the spacetime is allowed intrinsic curvature, while Minkowskian spacetime, technically, is the region of special relativity, which studies physical phenomena in a geometrically flat spacetime. Furthermore, the metric tensor in a Minkowski spacetime is often denoted by η_{ab}, and is defined explicitly below for Cartesian- (t, x, y, z) and spherical coordinates (t, r, θ, φ):

$$\eta_{ab} = \operatorname{diag}(-1, 1, 1, 1), \quad \text{for } x^a = (t, x, y, z); \tag{2.13}$$

$$\eta_{ab} = \operatorname{diag}(-1, 1, r^2, r^2 \sin(\theta)), \quad \text{for } x^a = (t, r, \theta, \varphi). \tag{2.14}$$

The indefinite property of the metric tensor in these spacetimes, by construction together with the axiom of the fixed speed of light in all reference systems, generates different classifications of spacetime vectors $v^a \in \mathcal{M}$. Each type of vector is used to span a surface known as the light cone, which describes the causal horizon of an observer at a point in space. To be more precise, the nature of a spacetime vector is determined by the inner product $\langle v|v\rangle$. The size of the light cone is restricted because the axiom of a fixed speed of light, or as it is sometimes known as the speed of causality.

For physicist it is often customary to denote the invariant infinitesimal distance squared $\mathrm{d}s^2$, between two vectors as

$$\mathrm{d}s^2 = g_{ab}\,\mathrm{d}x^a \mathrm{d}x^b. \tag{2.15}$$

This length or metric as physicists sometimes refer to it, is similar to the definition of a line element for a line integral

$$\int_\gamma f(\gamma)\,\mathrm{d}s = \int_\gamma f(\gamma)\,\sqrt{\mathrm{d}x^2 + \mathrm{d}y^2 + \mathrm{d}z^2}, \quad \gamma : \mathbb{R} \to \mathbb{R}^3, \;\&\; f : \mathbb{R}^3 \to \mathbb{R}. \tag{2.16}$$

By comparing the term for the line element in the integral and $\mathrm{d}s^2$, it is clear by inspection, that the metric tensor generalizes the notion of a line segment to more complex geometries. Another necessary definition is the length of a proper time interval, which relates to $\mathrm{d}s^2$ in the following manner,

$$\mathrm{d}\tau^2 = -\mathrm{d}s^2. \tag{2.17}$$

The metric is also able to generalize other geometrical quantities. One example is integral measures, for example $\mathrm{d}\mu = \mathrm{d}V$ is generalizable by employing the metric. An integral metric can be invariant to changes in coordinates. One example is a differential volume measure. We will define it by applying it for a region of spacetime $\Omega \subseteq \mathcal{M}$,

$$\int_\Omega f \,\mathrm{d}\mu = \int_\Omega f \sqrt{|\det(g_{ab})|}\mathrm{d}V = \int_\Omega f \,\sqrt{|g|}\mathrm{d}V, \tag{2.18}$$

where g acts as a shorthand notation for $\det(g_{ab})$.

3

Theory

3.1 Outline of the theory section

The purpose of this section is to introduce the reader to the major theoretical concepts applied in this work. At first, we will discuss the theory behind all tensors in the Einstein equation. After introducing the necessary tensors, we will briefly discuss the difficulties involved with finding general solutions to the Einstein equation and introduce the important Schwarzschild solution. After discussing the Einstein equation, we will start to discuss Dirac's equation and some of its properties. After introducing both the Dirac equation and the Einstein equations, we will conclude by introducing the Einstein-Dirac equation, by discussing its derivation and imposed boundary conditions.

3.2 Curvature tensors

This section will not generically define the necessary tensors describing the curvature of spacetime, instead we will only consider their tensor index representation, since this constitutes the minimal definitions required for defining the Einstein Equation. We begin with defining the tensors used in the left-hand side of the Einstein's equation, to do so, we first require an object which is not in general, a tensor object. In the literature it is known as the levi-cevita connection or Christoffel symbols. For our purposes, it is a (2,1)-tensor-like object, defined as follows [26]

$$\Gamma^{\delta}{}_{\alpha\beta} = \frac{1}{2} g^{\delta\sigma} \left[\frac{\partial g_{\sigma\alpha}}{\partial x^{\beta}} + \frac{\partial g_{\sigma\beta}}{\partial x^{\alpha}} - \frac{\partial g_{\alpha\beta}}{\partial x^{\sigma}} \right]. \tag{3.1}$$

Take note that it is constructed using first order differential operators acting on the metric tensor, $g_{\alpha\beta}$. Using the Christoffel symbols, we can define a new set of differential operators. One such operator is known as the covariant derivative D_{α},

$$D_{\alpha} V_{\beta} = \frac{\partial V_{\beta}}{\partial x^{\alpha}} - \Gamma^{\sigma}{}_{\alpha\beta} V_{\sigma}. \tag{3.2}$$

This operator is key to defining the notion of parallel transport of vector fields, as the Christoffel symbol considers any deviation of a vector's direction, as it is "transported" through an intrinsically curved space.

Using the covariant derivative and the Christoffel symbols, we can define the Riemann curvature tensor, by computing the commutator of the covariant derivative

(3.2), with two different indices, acting on a general covariant (1,0) tensor V_σ

$$\begin{aligned}[D_\alpha, D_\beta]V_\sigma &= D_\alpha(D_\beta V_\sigma) - D_\beta(D_\alpha V_\sigma) \\ &\overset{(3.2)}{=} \{\partial_\beta \Gamma^\delta_{\alpha\sigma} - \partial_\alpha \Gamma^\delta_{\beta\sigma} + \Gamma^\tau_{\alpha\sigma}\Gamma^\delta_{\tau\beta} - \Gamma^\tau_{\beta\sigma}\Gamma^\delta_{\tau\alpha}\}V_\delta.\end{aligned}$$

It is a quite lengthy computation but can be done by hand. As a result we can explicitly define the Riemann curvature tensor $R^\delta_{\alpha\beta\sigma}$, using the following equation

$$R^\delta_{\alpha\beta\sigma} := \partial_\beta \Gamma^\delta_{\alpha\sigma} - \partial_\alpha \Gamma^\delta_{\beta\sigma} + \Gamma^\tau_{\alpha\sigma}\Gamma^\delta_{\tau\beta} - \Gamma^\tau_{\beta\sigma}\Gamma^\delta_{\tau\alpha}. \tag{3.3}$$

Note that the Riemann tensor is a rank four tensor, and to be more precise it is a (3,1)-tensor. The tensor's components are constructed by derivatives of the Christoffel symbols (3.1), which in turn are constructed by derivatives of the metric tensor. Hence, we can claim that the Riemann tensor, is a tensor containing up to second order differential operators, acting on $g_{\mu\nu}$. To define Einstein's field equation, we require two lower order tensors, derived from the Riemann tensor. These are in order of tensor order, the Ricci tensor, and the curvature scalar. To obtain these tensors, we need to contract some, or all the indices in the Riemann tensor. At first, the Ricci tensor $R_{\mu\nu}$, is defined by contracting two indices, which reduces the corresponding tensor space from (3,1) to (2,0),

$$R^\delta_{\alpha\delta\sigma} = R_{\alpha\sigma}.$$

Finally, we will define the Ricci curvature scalar R. This scalar value is also known as the Ricci scalar, which, is a (0,0)-tensor. Construction the Ricci scalar requires a contraction operation on the Ricci tensor. To achieve this result, we must first multiply with a contravariant metric tensor. The introduced metric tensor, then allows for a final contraction, which effectively, removes any remaining indices.

$$R = g^{\alpha\sigma}R_{\alpha\sigma}.$$

3.3 The energy momentum tensor and energy conditions

A crucial part of Einstein's field equations is a term describing the flow and location of matter. Since axiomatically, the mere presence of matter in general relativity, causes the spacetime geometry to curve, as a response to its corresponding mass and energy. The tensorial object used to describe the mass and energy of any kind of matter, occupying a region of space time, is the stress-energy momentum tensor $T_{\mu\nu}$. Using this tensor, it is easy to write down a compact equation used to describe the conservation of mass and energy, namely $D_\mu T^{\nu\mu} = 0$. In spherical coordinates, the corresponding basis vectors $\{e_r, e_\theta, e_\varphi\}$, implies that the energy momentum tensor can be written on a diagonal form [15],

$$T^{\mu\nu} = \text{diag}(\rho, p_r, p_\perp, p_\perp). \tag{3.4}$$

The $T^{00} = \rho$ component, represents the energy density, $T^{11} = p_r$ denotes the radial pressure, and $T^{22} = T^{33} = p_\perp$ are the symmetrical tangential pressures. All the

described components are physical properties of the matter distribution, and thus play a central role in defining what are known as energy conditions. These conditions can be employed to test if the current matter model is physically sound, by properly conserving mass and energy. The standard energy conditions are in no particular order [15]

- The null energy condition (NEC): $\rho + p \geq 0$ where p is used to represent p_r or $p_\perp$.
- The weak energy condition (WEC): $\rho \geq 0$ in conjunction with the NEC condition.
- The dominant energy condition (DEC): $\rho - p \geq 0$ where p is used to represent p_r or $p_\perp$, this condition also requires the conditions from WEC.
- The strong energy condition (SEC): $\rho + p_r + 2p_\perp \geq 0$ together with NEC.

Beyond these conditions we will introduce another energy-like condition, which will be directly employed to study the Einstein-Dirac system. It is defined using the components outlined above.

$$p_r + 2p_\perp \leq \Omega \cdot \rho, \quad \text{where } \Omega \in \mathbb{R}_+ = \{x \in \mathbb{R} : \ x \geq 0\}. \tag{3.5}$$

There is no standard methodology for deriving $T^{\mu\nu}$, due to the physical association of the tensor. One method used to derive the tensor, applies methods from the calculus of variations, on the very popular action functional.

$$S(f) = \int_\Omega f \, \mathrm{d}x, \quad \forall f \in C^0, \ \Omega \subset \mathbb{R}^d.$$

For physical applications, the action functional is operating on the Lagrangian density, $\mathcal{L}_M = \sqrt{|g|} L_M$, where L_M represents a Lagrangian functional, defined by the matter model [26]. More explicitly, $S(\mathcal{L}_m)$ can be written as

$$S(\mathcal{L}_M) = \int_\Omega \mathcal{L}_M \, \mathrm{d}x = \int_\Omega L_m \sqrt{|g|} \, \mathrm{d}x, \quad \text{where } g = \det(g_{\mu\nu}) \ \& \ \Omega \subseteq \mathcal{M}. \tag{3.6}$$

Using this action, the elements of the energy momentum tensor, can be derived as follows [26]

$$T_{\mu\nu} = \frac{C_M}{8\pi} \frac{1}{\sqrt{|g|}} \frac{\delta S(\mathcal{L}_M)}{\delta g_{\mu\nu}}. \tag{3.7}$$

In the above equation, C_M is used the represent a constant which depends on the matter model, and $\delta S(\mathcal{L}_M)/\delta g_{\mu\nu}$ denotes the functional derivative, or variation of the action S, with respect to metric tensor's components.

3.4 Einstein's field equations

Einstein's equations or Einstein's field equations is a tensorial equation, which on the left-hand side is constructed by tensors describing the space time's curvature.

These are in order of occurrence, the Ricci-tensor $R_{\mu\nu}$, the Ricci-scalar R and the metric tensor $g_{\mu\nu}$. While the right hand side of the equation, is constructed using constants and the energy-momentum tensor $T_{\mu\nu} = g^{\mu\eta}g^{\nu\nu}T_{\eta\nu}$. Mathematically, the resulting equation, for a mostly positive metric signature, is defined as [27]

$$R_{\mu\nu} - \frac{1}{2}Rg_{\mu\nu} = 8\pi T_{\mu\nu}. \tag{3.8}$$

Due to the presence of the Ricci-tensor and scalar, it is in general, a second order, non-linear partial differential equation, describing the dynamics of the metric tensor's components. The resulting number of equations naturally depends on the dimension of the employed manifold and symmetry of the coordinate system. For physical applications, the spacetime is modelled using four dimensions, one time and three spatial dimensions, resulting in sixteen possible equations. Naturally, it follows that certain coordinate systems can reduce the number of independent equations. This effect is compounded when assuming that $g_{\mu\nu}$ is symmetric, which further reduces the number of equations to ten. The differential equations resulting from Einstein's field equations, are inherently complex, due to the complex definition of the curvature tensors, and the multitude of possible independent equations. Consequently, any general analytic solutions, are very difficult to find. Some of the most famous solutions are the Schwarzschild solution and the Kerr solution. The first named is important for the analysis performed in this thesis work, since it by construction, describes the geometry of a static spherically symmetric spacetime, outside a generating mass $M \in \mathbb{R}_+$. One important property of this solution is its asymptotic behavior far away from the mass, namely, asymptotic flatness. Physically, this formalizes the transition into a flat or non-curved spacetime, and mathematically, it can be formalized as follows.

$$\lim_{r\to\infty} g_{\mu\nu} = \eta_{\mu\nu}. \tag{3.9}$$

3.5 The Schwarzschild metric and compactness results

A very important, and historically influential solution, to the spherically symmetric static Einstein equations (3.8), is the well-known Schwarzschild metric [[18][26][27]]

$$g_{\mu\nu} = \operatorname{diag}\left(-\left(1-\frac{2M}{r}\right)^{-2}, \left(1-\frac{2M}{r}\right)^{-1}, r^2, r^2\sin^2(\theta)\right). \tag{3.10}$$

This metric has two important singularities at $r = 0$ and $r = 2M/r$. Where the latter is of great importance, since it used to define a metric known as the compactness of a solution to (3.8). This metric is characteristic of a particular solution to Einstein's equations and is defined by the ratio between the accumulated mass, up until a radius r, $m(r)$, and the radius r. For our analysis, the supremum of the quantity will act as our main metric,

$$\Gamma := \sup_{r>0} \frac{2m(r)}{r}. \tag{3.11}$$

The mass term, $m(r)$ is known as the quasi-local mass of a solution and is calculated by integrating the energy density ρ,

$$m(r) = \int_{\mathbb{R}^3} \rho(r)\, \mathrm{d}^3x = 4\pi \int_0^r s^2 \rho(s)\, \mathrm{d}s. \tag{3.12}$$

For highly compact solutions to (3.8), the value of Γ is very close to one. A historically significant result involving the compactness of some static, spherically symmetric solutions, to the Einstein equation, is known as the Buchdahl inequality [4]

$$\frac{2M}{R} < \frac{8}{9}. \tag{3.13}$$

At the left hand side of the inequality, M represents the total mass enclosed by the distribution ρ and R represents the smallest radius enclosing M, $m(R) = M$. The assumptions of the proof produced by H.A Buchdahl, assumes a few properties of ρ, among which is a non-increasing energy density, and isotropic pressure $p_r = p_\perp$. Both assumptions are not valid for the systems, which we will discuss in this thesis. A more general result was proved by Andréasson in 2008; this more general result does not require that ρ is strictly increasing.

Theorem 3.5.1 (Compactness bound [1]) *Let Ω, ρ and p_r be non-negative, and let the pressures $p_r, p_\perp$ and the energy density ρ satisfy*

$$\exists \Omega > 0 : \; p_r + 2p_\perp \leq \Omega \cdot \rho.$$

Then the following compactness bound holds

$$\sup_{r>0} \frac{2m(r)}{r} \leq \frac{(1+2\Omega)^2 - 1}{(1+2\Omega)^2}. \tag{3.14}$$

Note that this bound can reproduce Buchdahl's result, when $\Omega = 1$.

3.6 The Dirac equation

Schördinger's famous equation $\hat{H}\psi = i\frac{\partial \psi}{\partial t}$ was very influential during the evolution of quantum mechanics as a field of study. Written more explicitly, the equation is a parabolic partial differential equation.

$$i\frac{\partial \psi(\boldsymbol{x}, t)}{\partial t} - (\Delta + V)\, \psi(\boldsymbol{x}, t) = 0, \tag{3.15}$$

where Δ is Laplace operator and V is an unspecified potential. The initial strategy to derive a relativistic version of Schrödinger's equation involved including extra terms in the Hamiltonian, in a similar manner to perturbation theory. But the first truly relativistic quantum mechanical theory was provided by the Klein Gordon equation, which was derived by quantizing Einstein's energy, mass, and momentum relation.

$$E^2 = (mc^2)^2 + \|\boldsymbol{p}\|^2 c^2. \tag{3.16}$$

The Klein-Gordon equation did however display some inherent flaws. One important flaw is that the corresponding probability density $f_X = \Psi^*\Psi$, is not positive definite [20], as a result the axioms of probability theory is violated. Ergo, the Born rule, is unable to define a valid probability measure. This property, alongside the fact that the Klein-Gordon equation is only valid for spin zero particles (Bosons), motivated Paul Dirac among others, to find an equation to model spin 1/2 particles. In 1929 Dirac succeed and found an equation which later was named after him, the famous Dirac equation [23]

$$(i\not{D} - m)\Psi = 0.$$

The form given above is known as the free Dirac equation, where the included terms describe the momentum $\not{D}$ and the mass of the particle m. It is also possible to write in a more general form using the Hamiltonian formalism as $\hat{H}\Psi = E\Psi$, where $\hat{H} := -i\hbar c\boldsymbol{\alpha} \cdot \nabla + \beta m + V$ [23], but we will mostly concern ourselves with the more explicit from given above. The Dirac equation has since its invention been very successful. One such result, is the highly accurate prediction of the fine structure splitting of the energy levels in the hydrogen atom, which is one of the most accurate theoretical predictions in modern physics.

3.6.1 Derivation of the Dirac equation

In the following derivation, we will be considering a free particle (no potential, such as gravity or Coulomb potentials) moving in a Minkowski spacetime, which is the realm of special relativity. In this realm, the linear momentum $\boldsymbol{p}$, must be replaced by the four momentum $p^\mu = (E, \boldsymbol{p})$. All upcoming equations, and previous equations are formulated using natural units, furthermore $\eta_{\mu\nu} = \text{diag}(1, -1, -1, -1)$, will denote the Minkowski metric, with a mostly negative signature, in a $1 + 3$ spacetime. By contracting p^μ with p_μ we can rewrite equation (3.16), in terms of the four momentum,

$$p^\mu p_\mu = p^\mu \eta_{\mu\nu} p^\nu = E^2 - \|\boldsymbol{p}\|^2 \overset{(3.16)}{\Rightarrow} p^\mu p_\mu - m^2 = 0. \tag{3.17}$$

The final resulting equation $p^\mu p_\mu - m^2 = 0$, is the starting point used to derive the Dirac equation. If, we are able to factorize it, into two terms akin to the algebraic identity $(a^2 - b^2) = (a + b)(a - b)$, we would be able to define the Hamiltonian operator, using only one momentum operator. For this purpose, the equation needs to be reformulated, because the p^μ-term is a four vector, while m is a scalar. This is where Dirac's ingenuity started. He studied a general expression for the factorization and during the working procedure, decided what objects needed to be included into the equation for it to be well-posed. Thus, consider the final term in (3.17) and assume the following ansatz

$$p^\mu p_\mu - m^2 = (\alpha^\nu p_\nu + m)(\beta^\mu p_\mu - m). \tag{3.18}$$

The terms α^ν and β^μ, seems to at this stage, be some type of (0,1) tensor, in order for their contractions to be scalars. The components of each tensor object must be found such that the equality holds. By performing the multiplications and studying

the resulting terms, we find that

$$\alpha^\nu \beta^\mu p_\nu p_\mu - m\alpha^\nu p_\nu + m\beta^\mu p_\mu - m^2 = 0$$

$$\text{for } \mu = \nu \overset{(3.18)}{\Rightarrow} \alpha^\nu = \beta^\nu \text{ and since } p_\delta = p^\sigma \eta_{\delta\sigma} \Rightarrow \beta^\nu \beta^\mu p_\nu p_\mu - m^2 = 0.$$

The result in the final line is where Dirac discovered his famous gamma matrices. To make the remaining steps in the derivation towards the Dirac equation more explicit, let $\beta^\mu := \gamma^\mu$. Next, to define them, it is easier the make the summation over the indices more explicit and study the resulting terms,

$$\begin{aligned}\beta^\nu \beta^\mu p_\nu p_\mu - m^2 = {} & \gamma^0\gamma^0 p_0 p_0 + \gamma^0\gamma^1 p_0 p_1 + \gamma^0\gamma^2 p_0 p_2 + \gamma^0\gamma^3 p_0 p_3 \\ & + \gamma^1\gamma^0 p_1 p_0 + \gamma^1\gamma^1 p_1 p_1 + \gamma^1\gamma^2 p_1 p_2 + \gamma^1\gamma^3 p_1 p_3 \\ & + \gamma^2\gamma^0 p_2 p_0 + \gamma^2\gamma^1 p_2 p_1 + \gamma^2\gamma^2 p_2 p_2 + \gamma^2\gamma^3 p_2 p_3 \\ & + \gamma^3\gamma^0 p_3 p_0 + \gamma^3\gamma^1 p_3 p_1 + \gamma^3\gamma^2 p_3 p_2 + \gamma^3\gamma^3 p_3 p_3 - m^2.\end{aligned}$$

More compactly, we can rewrite them into two different contributions,

$$\beta^\nu \beta^\mu p_\nu p_\mu - m^2 = \sum_\mu \gamma^\mu\gamma^\mu p_\mu p_\mu + \sum_{\mu\neq\nu} (\gamma^\mu\gamma^\nu + \gamma^\nu\gamma^\mu) p_\nu p_\mu - m^2.$$

Some of the emergent terms appears to be an anticommutator between two matrices, that is $\{A, B\} = AB + BA$. This was a profound discovery since this implied that the solutions to the Dirac equation, are not scalar fields, as is the case with the Schrödinger equation. More on this later. By separately considering each term in the resulting equation, we find conditions that the γ^μ objects must satisfy. Starting with the first term. For the same indices the left hand side of equation (3.18) implies

$$\sum_\mu p^\mu p_\mu = \sum_{\mu,\nu} p^\mu \eta_{\mu\nu} p^\nu = \sum_{\mu=\nu} \gamma^\mu\gamma^\nu p_\mu p_\nu \Rightarrow \boxed{\gamma^\mu\gamma^\nu = \eta^{\mu\nu}}. \tag{3.19}$$

Due to this result and the fact that the terms from the second sum must vanish, we can ascertain another property of these Gamma matrices.

$$\sum_{\mu\neq\nu} (\gamma^\mu\gamma^\nu + \gamma^\nu\gamma^\mu) p_\nu p_\mu = \sum_{\mu\neq\nu} \{\gamma^\mu, \gamma^\nu\} p_\nu p_\mu = 0, \tag{3.20}$$

$$\text{by the definition of } \{\cdot,\cdot\},\ \eta_{\mu\nu} \text{ and (3.19)} \Rightarrow \boxed{\{\gamma^\mu, \gamma^\nu\} = 2\eta^{\mu\nu}.} \tag{3.21}$$

This result is important, as this defines the matrix representation of the Clifford algebra [23]. Hence, we can conclude that a more specific ansatz, which generates a correct factorization, is defined using γ^μ

$$p^\mu p_\mu - m^2 = (\gamma^\nu p_\nu + m)(\gamma^\mu p_\mu - m) = 0. \tag{3.22}$$

To end up with the Dirac equation, the final step is too exchange the four momentum p^μ with the differential operator $i\partial_\mu$. In quantum field theory the so called Feynman slash notation is used to denote the contraction of the γ^μ matrices and the operator ∂_μ, that is $\not{\partial} := \gamma^\mu \partial_\mu$. Finally, by applying the resulting operator on a wavefunction Ψ, we can write the Dirac equation for a free particle as follows.

$$(i\not{\partial} - m)\Psi = 0. \tag{3.23}$$

Since the Dirac equation is derived using the outlined factorization, there are solutions with both positive and negative energy, this is the main reason for the Dirac equation's predictions of anti-particles, such as the positron.

3.6.2 Dirac spinors and the gamma matrices

The wavefunction in the Dirac equation Ψ, is a four component spinor field $\Psi \in \mathbb{C}^4$, in contrast to the scalar wavefunction in Schrödinger's equation. The spinor fields, are elements of a special Hilbert space, namely, $\mathcal{H} = L^2(\mathbb{R}^3) \otimes \mathbb{C}^4$ [23]. The four spinor components, can be decomposed into two sets of spinor pairs ψ_A and ψ_B, meaning that we are able to compactly, write $\Psi = [\psi_A, \psi_B]^\top$. To study the properties of the two spinors, we use the unquantized free Dirac equation as a starting point,

$$(\gamma^\mu p_\mu - m)\phi = 0.$$

Above, $\phi = \phi(\boldsymbol{p})$, represents a generic four spinor. Performing a qualitative analysis, requires an explicit definition of the gamma matrices introduced during the derivation.

Definition 3.6.1 (Gamma and Pauli matrices [23]) *We will define the gamma matrices γ^μ, using both the Pauli matrices σ_i,*

$$\sigma_1 = \begin{bmatrix} 0 & 1 \\ 1 & 0 \end{bmatrix}, \quad \sigma_2 = \begin{bmatrix} 0 & -i \\ i & 0 \end{bmatrix}, \quad \sigma_3 = \begin{bmatrix} 1 & 0 \\ 0 & -1 \end{bmatrix},$$

and shorthand notations for the n-dimensional identity matrix and the n-dimensional "zero-matrix"

$$\boldsymbol{I}_n := \begin{bmatrix} 1 & 0 & \dots & 0 \\ 0 & 1 & \dots & 0 \\ \vdots & \vdots & \ddots & \vdots \\ 0 & 0 & \dots & 1 \end{bmatrix}, \quad \boldsymbol{0}_n := \begin{bmatrix} 0 & 0 & \dots & 0 \\ 0 & 0 & \dots & 0 \\ \vdots & \vdots & \ddots & \vdots \\ 0 & 0 & \dots & 0 \end{bmatrix}.$$

Next, using the Pauli matrices and the introduced notation, we define the gamma matrices as follows.

$$\gamma^0 := \begin{bmatrix} \boldsymbol{I}_2 & \boldsymbol{0}_2 \\ \boldsymbol{0}_2 & -\boldsymbol{I}_2 \end{bmatrix}, \quad \gamma^i := \begin{bmatrix} \boldsymbol{0}_2 & \sigma_i \\ -\sigma_i & \boldsymbol{0}_2 \end{bmatrix}, \quad \textit{where } i \in \{1,2,3\}. \tag{3.24}$$

After establishing the new notation and matrices, we turn to the equation yet again. Following with the convention in the derivation, we use the signature (+,-,-,-) for the metric and denote the four momentum by $p^\mu = (E, \boldsymbol{p})$.

$$\begin{aligned}(\gamma^\mu p_\mu - m\boldsymbol{I}_4)\phi &= (\gamma^0 E + \gamma^i \eta_{ij} p^j - m\boldsymbol{I}_4)\phi \quad (i \in \{1,2,3\}) \\ &= \begin{bmatrix} (E-m)\boldsymbol{I}_2 & -\boldsymbol{p}\cdot\sigma \\ \boldsymbol{p}\cdot\sigma & (-E-m)\boldsymbol{I}_2 \end{bmatrix} \phi.\end{aligned}$$

In the final matrix expression $\boldsymbol{p}\cdot\sigma$, represents the scalar matrix products $\boldsymbol{p}\cdot\sigma := \sum_{i=1}^3 p_i\sigma_i$. By decomposing the four spinor ϕ into $\phi = [\phi_A, \phi_B]^\top$, we can use the matrix equation to solve for a set of equations involving the spinor components

$$\begin{aligned}\phi_A &= \frac{\boldsymbol{p}\cdot\sigma}{E-m}\phi_B, \\ \phi_B &= \frac{\boldsymbol{p}\cdot\sigma}{E+m}\phi_A.\end{aligned}$$

Using this relation between the components, we are able to construct two sets of component pairings, by utilizing the fact that Einstein's energy momentum relation (3.16), mathematically, allows for both positive and negative energies. Indeed, $E = \pm\sqrt{m^2 + \|\boldsymbol{p}\|^2}$. In the case when considering positive energies $E > 0$, we can set ϕ_A to be the two component Pauli basis spinor e_i, where $i \in \{1, 2\}$ and $e_1 = [1, 0]^\top$, $e_2 = [0, 1]^\top$. Using the second equation we can define a set of positive energy spinors $\phi_i^{(+)}$, while the first equation for ϕ_A, can be used to define a set of spinors associated with negative energies $\phi_i^{(-)}$. Explicitly we can write them as follows [16]

$$\phi_i^{(+)} = \begin{bmatrix} e_i \\ \frac{\boldsymbol{p}\cdot\boldsymbol{\sigma}}{E+m} e_i \end{bmatrix}, \quad \phi_i^{(-)} = \begin{bmatrix} -\frac{\boldsymbol{p}\cdot\boldsymbol{\sigma}}{E+m} e_i \\ e_i \end{bmatrix}. \tag{3.25}$$

We can also define a new set of spinors $\xi_i(\boldsymbol{p}) = \varepsilon^{ij}\phi_j^{(-)}(-\boldsymbol{p})$, where ε^{ij} is a rank two Levi-Civita tensor. Given the positive- and the new negative energy spinor field, we can show the final claim from the derivation, that is each factor in (3.18), is associated with either positive or negative energy solutions [16]

$$\begin{aligned} &\text{for, } E > 0: \quad (\gamma^\mu p_\mu - m)\phi_i^{(+)}(\boldsymbol{p}) = 0, \\ &\text{for, } E < 0: \quad (\gamma^\mu p_\mu + m)\xi_i(\boldsymbol{p}) = 0. \end{aligned}$$

The complete four spinor Dirac wavefunction for a free particle, is summarized below,

$$\Psi(x, \boldsymbol{p}) = C \begin{cases} \phi_i^{(+)}(\boldsymbol{p}) e^{-i\boldsymbol{p}\cdot\boldsymbol{x}} \text{ when } E > 0 \\ \xi_i(\boldsymbol{p}) e^{i\boldsymbol{p}\cdot\boldsymbol{x}} \text{ when } E < 0. \end{cases}, \quad C \in \mathbb{R}. \tag{3.26}$$

Finally, we will discuss the relative amplitude between the two spinor fields. At first, note that the fractions in front of the Pauli basis spinors e_i, in equation (3.25), implies an asymmetry for the amplitudes [16]. For particles moving at non-relativistic speeds, the difference in amplitude due to fractions are greater. Due to this fact, the two spinor components are known as the small and large component, respectively. Furthermore, the nature of this asymmetry, will be more or less pronounced depending on the employed basis.

3.7 The Einstein-Dirac equations

The purpose of this section is to provide a background to the Einstein-Dirac equations. The first part of this section discusses the necessary derivation, while the second section summarizes the resulting set of equations and the imposed boundary conditions. The third and final subsection, discusses the process of defining initial conditions and presents the conditions applied for all results presented in this work.

3.7.1 Deriving the Einstein-Dirac equations

The original derivation made by Finster, Smoller and Yau in [10], is quite lengthy and is thus worth reading in their paper. But to justify the construction of the resulting equations, we will discuss the important steps in their derivation. The original

derivation was made by considering a single shell configuration which was occupied by two fermions with opposite spin states $s_1 = 1/2$, $s_2 = -1/2$ and total angular momentum j_1, j_2. The total angular momentum for a quantum state determines the angular structure of the resulting wave functions. In the case of the hydrogen atom, a state with angular momentum $l = 0$, yields a spherically symmetric wavefuntion [12],[20]. In literature about quantum mechanics, configurations with zero total angular momentum $j = l + s = 0$, are known as singlett states. A first key observation in order to be able generalize the original derivation for an arbitrary, even number of fermions κ, is to impose that $\kappa = 2j_{\max} + 1$, since the particles are fermions, this imposes that $j = (2n + 1)/2$ where $n \in \mathbb{N}$. Hence, by assuming that all fermions are uncharged, with spin equal to 1/2, we can occupy a single shell with the total number of fermions being equal to κ. This singlett configuration, is then used for the derivation of the Einstein-Dirac equations.

In order to derive the Einstein-Dirac system we first need to modify the Dirac operator we derived in Section 3.6.1. In particular, the assumption of a static Minkowski metric $\eta_{\mu\nu}$, is no longer of use and henceforth, a Dirac operator $\not{D}$ constructed using a general Lorentzian metric $g_{\mu\nu}$ is required. To this end, the more general expression for a Dirac operator $\not{D} = \gamma^\mu \partial_\mu + B$ is employed [10]. Remember that γ^μ, was previously constructed using $\eta_{\mu\nu}$, this implies that new gamma matrices, and an expression for B, is required. Finster, Smoller and Yau, employed the fact that the new γ^μ matrices can be formed using a linear combination of the old gamma matrices, defined in Section 3.6.2. Using a similar argument, we also require an equivalent anticommutator relation $\{\gamma^\mu, \gamma^\nu\} = 2g^{\mu\nu}$. Since we also employ another coordinate system, we also require a transformation of the Pauli matrices into spherical coordinates (t, r, θ, φ). This transformation yielded three new matrices, $\sigma_r(r, \theta, \varphi)$, $\sigma_\theta(r, \theta, \varphi)$ and $\sigma_\varphi(r, \theta, \varphi)$. To perform a tensor transformation of σ_i, and to compute the curvature tensors, we require an ansatz for the metric tensor.

$$g_{\mu\nu} = \operatorname{diag}\left(-\frac{1}{T^2(r)}, \frac{1}{A(r)}, r^2, r^2\sin^2(\theta)\right), \quad r > 0,\ \theta \in [0, \pi],\ \varphi \in [0, 2\pi]. \tag{3.27}$$

After constructing a new Dirac operator, a plane wave ansatz for each four-spinor wave function is made,

$$\Psi_a = T(t; \omega) f(r, \theta, \varphi) = e^{-i\omega t}\frac{\sqrt{T}}{r}\begin{bmatrix} \Phi_1 e_a \\ i\sigma_r \Phi_2 e_a \end{bmatrix}, \tag{3.28}$$

similar to the argumentation in Section 3.6.2, e_a is assumed to be a basis. Due to the plane wave ansatz, the time dependence is encoded in a separable factor $\exp(-i\omega t)$, where $\omega \overset{\hbar=1}{=} E$ is both the oscillation frequency and the eigenvalue/ energy for a state Ψ_{jk} ($\hat{H}\psi = E\psi$). The lower indices j are k are quantum numbers for a certain state, j is the total angular momentum and k is the magnetic quantum number [12].

To construct static and spherically symmetric solutions, requires that f can be factorized, $f(r, \theta, \varphi) = R(r)\Theta(\theta, \varphi)$. For this purpose, a basis is constructed using a linear combination of the spherical harmonics function and the standard basis e_a

of $\mathbb{R}^2$ [[5] [8] [14]]. To follow the notation used by the authors, we also set $\Phi_1 = \alpha$ and $\Phi_2 = \beta$, using this notation and the described basis, the resulting ansatz for one wave function becomes

$$\psi_{jk} = e^{-i\omega t}\frac{\sqrt{T(r)}}{r}\begin{bmatrix}\chi^k_{j-1/2}\alpha(r)\\ i\chi^k_{j+1/2}\beta(r)\end{bmatrix}. \tag{3.29}$$

The χ-terms, are used to denote a basis, constructed by a linear combination of e_1 and e_2 and the spherical harmonics function $Y^a_b = Y^a_b(\theta,\varphi)$ (for a explicit definition see for example [12] or [20]),

$$\chi^k_{j-1/2} = \sqrt{\frac{j+k}{2j}}Y^{k-1/2}_{j-1/2}e_1 + \sqrt{\frac{j-k}{2j}}Y^{k+1/2}_{j-1/2}e_2,$$
$$\chi^k_{j+1/2} = \sqrt{\frac{j+1-k}{2j+2}}Y^{k-1/2}_{j+1/2}e_1 - \sqrt{\frac{j+1+k}{2j+2}}Y^{k+1/2}_{j+1/2}e_2.$$

It was shown by Finster, Smoller and Yau, that the effective wave function for our singlett state with $\kappa = 2j+1$ particles, using the previous plane wave ansatz with the spherical harmonics, includes an extra factor of κ [8]. The resulting wavefunction spinor therefor has an explicit dependence on κ, and this simplifies the construction of systems with increasing number of particles. Furthermore, the Dirac equation can be reduced into a set of two equations describing the two spinor components $\Phi = [\alpha,\beta]^\top$ and the metric fields A, T [8]

$$\left(\omega T\begin{bmatrix}1 & 0\\ 0 & -1\end{bmatrix} + \sqrt{A}\frac{\partial}{\partial r}\begin{bmatrix}0 & 1\\ 1 & 0\end{bmatrix} + \frac{\kappa}{2r}\begin{bmatrix}0 & -1\\ 1 & 0\end{bmatrix} - m\boldsymbol{I}_2\right)\Phi = 0. \tag{3.30}$$

The resulting equation is real, and as a result, we can conclude that α and β are real valued maps. Next, for the α and β fields to define a physical wave function, they must be normalisable with respect to some inner product $\langle\cdot|\cdot\rangle$. The required inner product is identifiable by requiring that $\not{D}$ is self-adjoint with respect to it. After identifying the inner product, the corresponding normalization condition for α and β can be written as [10],

$$\langle\Psi|\Psi\rangle = 4\pi\int_0^\infty(\alpha^2(r)+\beta^2(r))\frac{T(r)}{\sqrt{A(r)}}\,\mathrm{d}r = 1. \tag{3.31}$$

So far, we have achieved two equations and one boundary condition, what remains is to identify two extra equations by using Einstein's equations (3.34). The left hand side of the Einstein equations, are long standard computations, while the right hand side requires formulating the energy momentum tensor $T_{\mu\nu}$. The components of the energy momentum tensor can be identified using a matter action (3.7). To define the matter action for the Dirac equation, we first require the Lagrangian density of the Dirac equation [16]

$$\mathcal{L}_M = \bar{\Psi}(i\not{D} - m)\Psi\sqrt{|g|} = \Psi^\dagger\gamma^0(i\not{D} - m)\Psi\sqrt{|g|},$$

where g is the determinant of the metric $g = \det(g_{\mu\nu})$ and $\Psi^\dagger$ denotes the conjugate transpose of Ψ. Using this Lagrangian density, the corresponding matter action becomes

$$S(\mathcal{L}_M) = \int_{\mathcal{M}} \Psi^\dagger \gamma^0 (i\not{D} - m)\Psi \sqrt{|g|}\, \mathrm{d}^4x.$$

Finally, by computing the variation of S with respect to $g_{\mu\nu}$, the energy momentum tensor follows as a result. To summarize all results, the Einstein equations, yields two more independent equations,

$$rA' = 1 - A - 8\pi\kappa\omega T^2(\alpha^2 + \beta^2), \tag{3.32}$$

$$2rA\frac{T'}{T} = A - 1 - 8\pi\kappa\omega T^2(\alpha^2 + \beta^2) + 8\pi\frac{\kappa^2}{r}T\alpha\beta + 8\pi\kappa m T(\alpha^2 - \beta^2). \tag{3.33}$$

In the equation above, the notation A' and T', denotes the derivative with respect the radial variable r, $T'(r) = \frac{\mathrm{d}}{\mathrm{d}r}T(r)$ and $A'(r) = \frac{\mathrm{d}}{\mathrm{d}r}A(r)$.

3.7.2 Summarizing the Einstein-Dirac equations

After minimizing the Dirac matter action ($S(\mathcal{L}_M)$) and deriving the Dirac differential operator $\not{D}$, we get a system of four, coupled ordinary differential equations (ODEs), describing the Fermion fields $\alpha = \alpha(r)$, $\beta = \beta(r)$ and the metric fields $A = A(r)$, $T = T(r)$

$$\alpha' = \frac{\kappa}{2}\frac{\alpha}{r\sqrt{A}} - (\omega T + m)\frac{\beta}{\sqrt{A}}, \tag{3.34a}$$

$$\beta' = (\omega T - m)\frac{\alpha}{\sqrt{A}} - \frac{\kappa}{2}\frac{\beta}{r\sqrt{A}}, \tag{3.34b}$$

$$A' = \frac{1}{r} - \frac{A}{r} - 8\pi\kappa\omega\frac{T^2}{r}(\alpha^2 + \beta^2), \tag{3.34c}$$

$$T' = \frac{T}{2r} - \frac{T}{2rA} - 4\pi\kappa\omega\frac{T^3}{rA}(\alpha^2 + \beta^2) + 4\pi\kappa^2\frac{T^2}{r^2A}\alpha\beta + 4\pi\kappa m\frac{T^2}{rA}(\alpha^2 - \beta^2). \tag{3.34d}$$

The solutions to the Einstein-Dirac equations must satisfy a few conditions to be physically significant. These imposed requirements, for all included fields, turns the system of differential equations into a boundary value problem. Where we have regularity requirements at $r = 0$, and physically motivated asymptotic behavior.

- The fermion fields must be normalisable with respect to the inner product

$$\langle \psi, \psi \rangle = 4\pi \int_0^\infty (\alpha^2 + \beta^2)\frac{T}{\sqrt{A}}\, \mathrm{d}r = 1. \tag{3.35}$$

- The metric fields should be asymptotically flat,

$$\lim_{r\to\infty} A(r) = \lim_{r\to\infty} T(r) = 1. \tag{3.36}$$

More details about the equations will follow in the method section, but there is still one important set of conditions we must specify and those are the initial values for all fields.

3.7.3 Initial conditions for the Einstein-Dirac equations

The solution sets to the Einstein-Dirac equations which are physically interesting are non-singular at the origin. Which necessitates the introduction of well-defined initial conditions, and since the equations are of first order, it is only necessary to specify conditions for the fields without any derivatives. To avoid any emergent singularities, close to the origin requires that conditions must be imposed for small radii. To this end, we employ a truncated Maclaurin series expansion, using a general ansatz for each field in (3.34),

$$f(x) \approx \sum_{j=1}^{N} c_j x^j, \quad N \geq 1. \tag{3.37}$$

The sum contains only finitely many terms, since the contributions from higher order terms will diminish, as the expansion is only applied to a small neighborhood around $r = 0$. Meaning effectively that the number of coefficients c_j and the highest order N of r must be determined using the resulting system of equations. This also implies that the resulting initial conditions, are not necessarily unique. The set of initial conditions applied for this work, was selected to coincide with Leith et. al [14]:

$$\alpha(r) = \alpha_1 r^{\kappa/2} + \mathcal{O}(r^{(\kappa/2+2)}), \tag{3.38a}$$

$$\beta(r) = \frac{1}{\kappa+1}(\omega T_0 - m)\alpha_1 r^{(\kappa/2+1)} + \mathcal{O}(r^{(\kappa/2+3)}), \tag{3.38b}$$

$$A(r) = 1 - 8\pi\omega T_0^2 \alpha_1^2 \frac{\kappa}{\kappa+1} r^{\kappa} + \mathcal{O}(r^{(\kappa+2)}), \tag{3.38c}$$

$$T(r) = T_0 - 4\pi T_0^2 \alpha_1^2 \frac{1}{\kappa+1}(2\omega T_0 - m) r^{\kappa} + \mathcal{O}(r^{(\kappa+2)}). \tag{3.38d}$$

This set of initial conditions introduces two new parameters T_0 and α_1. Where the first parameter, denotes the value of the T-metric field at the origin, $T_0 = T(r)|_{r=0}$, and the final parameter α_1, denotes the slope of the fermion field, also in the origin,

$$\alpha_1 = \frac{\mathrm{d}}{\mathrm{d}r}\alpha(r)\bigg|_{r=0}. \tag{3.39}$$

While solving the Einstein-Dirac equations numerically, we must a priori, choose values for these parameters.

3.8 Energy density and matter pressure functions for the Einstein-Dirac system

The fermion- and metric fields as described by the Einstein-Dirac equations, gives rise to some emergent matter properties, and these are the matter distribution ρ and matter pressure components generated by matter ensembles p_r and $p_\perp$. The functional form for each matter property, can be identified directly from the energy

momentum tensor as was outlined in section 3.3, or by identifying terms from the Einstein equations without performing the derivation, which requires knowledge of $R_{\mu\mu}$ and R,

$$R_{00} + \frac{1}{2}Rg_{00} = 8\pi\rho,$$
$$\frac{1}{r}A'(r) - \frac{1}{r^2} + A(r) = 8\pi\left\{\kappa\omega\left(\frac{T(r)}{r}\right)^2(\alpha^2(r) + \beta^2(r))\right\}$$

In the following definition, we will define all three matter property functions, the energy density ρ, the radial pressure p_r and the tangential pressure $p_\perp$.

Definition 3.8.1 (Matter property functions [10][14]) *Let α and β be Dirac fields, furthermore, let A and T be metric fields from the Einstein-Dirac equations* (3.34)*. Then we define the energy density function $\rho(r)$, the radial pressure function $p_r(r)$ and the tangential pressure function $p_\perp(r)$ by*

$$\rho(r) = \kappa\omega\frac{T^2(r)}{r^2}(\alpha^2(r) + \beta^2(r)),$$
$$p_r(r) = \kappa\frac{T(r)}{r^2}\left[\omega T(r)(\alpha^2(r) + \beta^2(r)) - m(\alpha^2(r) - \beta^2(r)) - \kappa\frac{\alpha(r)\beta(r)}{r}\right],$$
$$p_\perp(r) = \frac{\kappa^2}{2r^3}T(r)\alpha(r)\beta(r).$$

3.9 Gravitationally induced redshift

A measure of how strong the gravitational field which emerges from the curved space time $(\mathcal{M}, g)$, is known as the gravitational redshift z. To be more precise it is an emergent phenomenon from the time-dilation effects encoded by the metric g. The effect is typically measured as a decrease in the frequency of light, which can be expressed using the following equation [27]

$$z + 1 = \frac{f_{em}}{f_{ob}}, \tag{3.40}$$

where f_{em} and f_{ob} is the emitted and observed frequency, respectively. The redshift z, can be derived by considering a static in space, spacetime curve $\gamma^\mu(t) = (t, r, \theta, \varphi)$ where $t \in [t_0, t_1]$ and the remaining variables are constants. The length of a proper-time interval $\Delta\tau$, is by definition,

$$\Delta\tau \triangleq \int_\gamma \mathrm{d}\tau = \int_\gamma \sqrt{-g_{\mu\nu}\mathrm{d}x^\mu\mathrm{d}x^\nu} \tag{3.41}$$
$$= \int_{t_0}^{t_1}\sqrt{-g_{\mu\nu}\frac{\mathrm{d}x^\mu}{\mathrm{d}t}\frac{\mathrm{d}x^\nu}{\mathrm{d}t}}\,\mathrm{d}t \tag{3.42}$$

Inserting the metric ansatz for the Einstein-Dirac equations (3.27) into the integral yields,

$$\Delta\tau = \int_{t_0}^{t_1} \sqrt{-g_{00}\left(\frac{\mathrm{d}}{\mathrm{d}t}(t)\right)^2 - g_{11}\left(\frac{\mathrm{d}}{\mathrm{d}t}(r)\right)^2 + \dots}\ \mathrm{d}t \tag{3.43}$$

$$= \int_{t_0}^{t_1} \sqrt{-g_{00}}\,\mathrm{d}t = \int_{t_0}^{t_1} T(r)^{-1}\,\mathrm{d}t \overset{r \text{ is constant}}{=} T(r)^{-1}\Delta t, \quad (\Delta t := t_1 - t_0). \tag{3.44}$$

Which implies that $\Delta\tau/\Delta t = T(r)^{-1}$. In order to apply (3.40) to the previous result, we must first note that the frequency f, of a beam of light, is inversely related to time $f = 1/t$. Given this physical fact, we can associate the emitted frequency with $\Delta\tau$, and the observed frequency with Δt and conclude that,

$$z + 1 = \frac{f_{em}}{f_{ob}} = \left(\frac{\Delta\tau}{\Delta t}\right)^{-1} = T(r) \Leftrightarrow z = T(r) - 1 \quad \square. \tag{3.45}$$

A final remark. This result holds for a general value of r, but the redshift values which are of main interest to classify the apparent relativistic nature of the Einstein-Dirac solutions (α, β, A, T), is the central redshift. Which we will define as

$$z := T(r)|_{r=0} - 1 \overset{(3.38)}{=} T_0 - 1. \tag{3.46}$$

3.10 An introduction to the Einstein-Vlasov system

The objective of kinetic theory is to describe ensembles of particles using macroscopic distributions. Where the particles from the ensembles are interacting with each other with some kind of force, for example, in case of an electron cloud or a collection of charged particles, the dominating interaction is assumed to be the Lorentz force. A classic example of a particle distribution is the Maxwell Boltzmann distribution, which is used to describe the distribution of velocities of particles in an ideal gas. Turning towards the Einstein-Vlasov system, it is relativistic matter model where the matter ensemble is described by a position and momentum matter distribution in phase space. The distribution function is defined using a collision-less Boltzmann distribution equation, which for the static case $f = f(\boldsymbol{x}, \boldsymbol{v})$ reads

$$v^\mu \frac{\partial}{\partial x^\mu} f + F^\mu \frac{\partial}{\partial v^\mu} f = 0,$$

where $\boldsymbol{F} \in \mathbb{R}^3$ is the force interaction between the particles, which for the Einstein-Vlasov model is a gravitational force provided by Einstein's equations. For the spherically symmetric static/ steady state Einstein-Vlasov system the metric tensor is assumed to be defined by the ansatz [2],

$$g_{\mu\nu} = \mathrm{diag}\left(-e^{2\mu(r)}, e^{2\lambda(r)}, r^2, r^2\sin^2(\theta)\right), \quad r > 0,\ \theta \in [0, \pi],\ \varphi \in [0, 2\pi], \tag{3.47}$$

and similarly to the Einstein-Dirac system, it is described by a system of differential equations where a subset is generated from the matter content and the rest are

directly defined from the Einstein-equations (3.8). Before writing the Einstein-Vlasov equations we will denote the matter distribution in spherical coordinates by $f = f(r, w, L)$, here w, L represents angular momentum variables where $w \in \mathbb{R}$ and $L \in \mathbb{R}_+$ ($\mathbb{R}_+ = \{x \in \mathbb{R} : x \geq 0\}$). The differential equations describing the Einstein-Vlasov system is defined explicitly in the following equation [3]

$$w\,\partial_r f - \left(\left(1 + w^2 + \frac{L}{r^2}\right)\mu' - \frac{L}{r^3}\right)\partial_w f = 0 \tag{3.48a}$$

$$e^{-2\lambda}(2r\lambda' - 1) + 1 = 8\pi r^2 \rho, \tag{3.48b}$$

$$e^{-2\lambda}(2r\mu' + 1) - 1 = 8\pi r^2 p_r, \tag{3.48c}$$

$$e^{-2\lambda}(\mu''(\mu + \frac{1}{r})(\mu' - \lambda')) = 8\pi p_\perp. \tag{3.48d}$$

The boundary conditions are presented below.

- Non-singular center,

$$\lambda(r)|_{r=0} = 0 \text{ and } \mu(r)|_{r=0} = \mu_0 \in \mathbb{R}. \tag{3.49}$$

- Asymptotically flat metric functions

$$\lim_{r\to\infty} \lambda(r) = \lim_{r\to\infty} \mu(r) = 0 \Rightarrow g_{\mu\nu} \to \eta_{\mu\nu} \text{ as } r \to \infty. \tag{3.50}$$

The energy momentum tensor is diagonal due to the spherical coordinate system (3.4), and similarly to the Einstein-Dirac system in Section 3.8, we can define the matter quantity functions using the metric- and the distribution functions.

Definition 3.10.1 (Matter property functions [3]) *Let w, L be the radial component in the angular momentum and the angular momentum squared, respectively. Also let $f = f(r, w, L)$ be the matter distribution function $f : \mathbb{R} \times \mathbb{R}_+ \times \mathbb{R}_+ \to \mathbb{R}$. Then we define the energy density function $\rho(r)$, the radial pressure function $p_r(r)$ and the tangential pressure function $p_\perp(r)$ by*

$$\rho(r) = \frac{\pi}{r^2}\int_{\mathbb{R}}\int_{\mathbb{R}_+} f\sqrt{1 + w^2 + \frac{L}{r^2}}\,\mathrm{d}L\,\mathrm{d}w,$$

$$p_r(r) = \frac{\pi}{r^2}\int_{\mathbb{R}}\int_{\mathbb{R}_+} \frac{w^2}{\sqrt{1 + w^2 + \frac{L}{r^2}}} f\,\mathrm{d}L\,\mathrm{d}w,$$

$$p_\perp(r) = \frac{1}{2}\frac{\pi}{r^4}\int_{\mathbb{R}}\int_{\mathbb{R}_+} \frac{L}{\sqrt{1 + w^2 + \frac{L}{r^2}}} f\,\mathrm{d}L\,\mathrm{d}w.$$

It can be shown that a family of static spherically symmetric solutions, can be produced using an ansatz $f = \Phi(E, L)$ [2]. Where E is physical quantity which has been shown to be conserved in spherical coordinate systems [2], and is defined below

$$E = e^{\mu(r)}\sqrt{1 + w^2 + \frac{L}{r^2}}.$$

To be more specific we will employ what is known as the polytropic ansatz, for the distribution function f. We will write it explicitly using the max function $(x)_+ = \max\{0, x\}$ [2]

$$f(r, w, L) = \left(1 - \frac{E}{E_0}\right)_+^k (L - L_0)_+^l, \tag{3.51}$$

where $E_0 > 0$ is a strictly positive parameter and L_0 is a positive parameter, the final two parameters are assumed to obey $l > -1/2$ and $k > -1$. For numerical purposes we also introduce a function involving the metric function μ, $y(r) = e^{\mu(r)}/E_0$, while computing the Vlasov system's density we also require the value of this function at the origin, $y_0 = y(0) = e^{\mu(0)}/E_0$. For more details, the interested reader is refereed to [2].

4

Methods

4.1 Overview

The set of Einstein-Dirac equations is a system of coupled non-linear differential equations, meaning that analytic solutions are difficult to find. Due to the nature of the problem the equations are effectively a boundary value problem, with conditions on both the fermion fields and the metric fields, see Section 3.7.2. The fermion fields represented by $\alpha(r)$ and $\beta(r)$ are elements of $L^2(\mathbb{R})$, and must therefore exhibit a decay behavior such that $\alpha(r), \beta(r) \to 0$ as $r \to \infty$. In addition, the metric fields A and T, should instead converge to one. This condition is formally known as asymptotic flatness. Due to symmetry and the static nature of the problem all metric fields should intersect with the Schwarzschild solution (3.10) while converging towards the Minkowski metric, $g_{\mu\nu} \to \eta_{\mu\nu}$ as $r \to \infty$, where $\eta_{\mu\nu} = \text{diag}(-1, 1, r^2, r^2 \sin^2(\theta))$. Numerically both conditions are very difficult to satisfy due to the inherent limitations of floating-point numbers, which necessitates a different approach to the problem.

Solving the system boils down to a few key steps.

- First, we must initialize values for the system's parameters, they are in no particular order, m, ω and κ for the ODEs (3.34), and T_0, α_1 for the initial conditions (3.38).
- After fixing these parameters the system should be solved using relaxed constraints for all fields.
- If the conditions are satisfied, the resulting solutions must be scaled in order for them to be physically relevant.

The main difficulty of the problem originates from the nature of quantum mechanical systems. For the boundary conditions to be satisfied, we require a very particular value for ω, since it is a physical parameter which is proportional to the energy level for a certain quantum state. The discrete nature of energy levels for quantum states originates from the postulate of quantized observables [6]. The identification of the specific ω parameter, using numerical methods, requires repeatedly solving the ODEs while updating ω, until the relaxed conditions are satisfied. This type of solution methodology is generally known as a shooting method. More details about all methods and their implementations can be found in their relevant sections.

4.2 Relaxing the boundary conditions and scaling the equations

As was previously discussed, a numerical treatment of the Einstein-Dirac equations requires that the boundary conditions are relaxed, (3.35) and (3.36). The new relaxed boundary conditions are instead,

$$4\pi \int_0^\infty (\alpha^2 + \beta^2) \frac{T}{\sqrt{A}} \, \mathrm{d}r < \infty, \tag{4.1}$$

$$\lim_{r\to\infty} A(r) < \infty, \quad \lim_{r\to\infty} T(r) < \infty. \tag{4.2}$$

Both conditions was applied in order to define two scaling factors λ and τ, in accordance with the methodology introduced by Finster, Smoller and Yau [10]

$$\lambda := \left(4\pi \int_0^\infty (\alpha^2 + \beta^2) \frac{T}{\sqrt{A}} \, \mathrm{d}r \right)^{1/2}, \quad \tau := \lim_{r\to\infty} T(r). \tag{4.3}$$

These parameters are calculated and applied after a set of solutions (α, β, A, T) to the relaxed problem are found, in order to generate a second set of scaled solutions $(\tilde{\alpha}, \tilde{\beta}, \tilde{A}, \tilde{T})$. The set of unscaled - and scaled functions, are defined as follows.

Definition 4.2.1 *We will define the set of unscaled solutions,* (α, β, A, T)*, as a set consisting of four sequences* $\{\{\alpha_i\}_{i=0}^N, \{\beta_i\}_{i=0}^N, \{A_i\}_{i=0}^N, \{T_i\}_{i=0}^N\}$*, which satisfies* (4.1) *and* (4.2) *where* $N \in \mathbb{N} \setminus \{0\}$*. Given a set of unscaled solutions,* (α, β, A, T)*, we also define its corresponding parameter set* $\{\lambda, \tau\}$ *by* (4.3)*. Finally, we define the set of scaled metric- and fermion fields* $(\tilde{\alpha}, \tilde{\beta}, \tilde{A}, \tilde{T})$*, using* (α, β, A, T) *and* $\{\lambda, \tau\}$*, as*

$$\begin{aligned}
&\tilde{A}(r) := A(\lambda r), \quad \tilde{T}(r) := \frac{1}{\tau} T(\lambda r), \\
&\tilde{\alpha}(r) := \sqrt{\frac{\tau}{\lambda}} \alpha(\lambda r), \quad \tilde{\beta}(r) := \sqrt{\frac{\tau}{\lambda}} \beta(\lambda r), \\
&(\tilde{\alpha}, \tilde{\beta}, \tilde{A}, \tilde{T}) := \left\{ \{\tilde{\alpha}_i\}_{i=0}^N, \{\tilde{\beta}_i\}_{i=0}^N, \{\tilde{A}_i\}_{i=0}^N, \{\tilde{T}_i\}_{i=0}^N \right\}.
\end{aligned}$$

Inserting the scaled fields into (3.34), the resulting set of equations are the same, but differs only by two re-scaled parameters $\omega \to \tilde{\omega}$ and $m \to \tilde{m}$. Both of the new parameters are defined by the parameter set $\{\lambda, \omega\}$,

$$\tilde{\omega} := \lambda \omega \tau, \quad \tilde{m} := \lambda m. \tag{4.4}$$

For an explicit derivation, see Appendix A.1. The new parameters are important, since they constitute the physically correct frequency of oscillation of the wavefunctions and the effective mass of the fermions, respectively. Furthermore, the initial value parameters in (3.38), for the unscaled solutions are not the same in the scaled case due to the introduced constants in front of the scaled function $(\tilde{\alpha}, \tilde{\beta}, \tilde{A}, \tilde{T})$. However, it is sufficient to identify what the scaled version of T_0 should be, since this defines the apparent red-shift of the solutions, $z = T_0 - 1$, see Section 3.9. Since it is simply the value of the field at the origin, we can approximate it using the smallest initial value from the integration, $T_0 \approx T(r_{\min})$.

4.3 Computing the scaling parameters

In this section we will discuss the methods employed to compute the parameter set $\{\lambda, \tau\}$ from a set of unscaled solutions (α, β, A, T). We will start by discussing the computation of λ, recall that it was defined using an integral

$$\lambda = \left(4\pi \int_0^\infty (\alpha^2(r) + \beta^2(r)) \frac{T}{\sqrt{A}} \, \mathrm{d}r\right)^{1/2}.$$

This integral was computed using a composite trapezoidal rule, available in the integration subpackage of the `SciPy` library [25]. For numerical methods it is impossible to compute improper integrals, but since the fermion fields must decay, we can note that the contributions of the integrand to the total integral will diminish, and if the field is sufficiently close to zero, we can for our purposes ignore the extra contribution provided by integrating to infinity. The error of the approximation inherent to the trapezoidal rule, also referred to as the remainder, can be shown to be bounded by the following inequality [7]

$$|R(f, I_h)| \leq \frac{1}{12} \|f''\|_\infty \sum_{i=0}^{n-1} h_i^3.$$

Where $f : [a, b] \to \mathbb{R}$ is assumed to be twice differentiable on a closed interval $[a, b]$ where $a, b \in \mathbb{R}$. The norm $\|\cdot\|_\infty$ is the regular max norm, $\|f\|_\infty = \max_x |f(x)|$ and h_i is the distance between samples. The arguments in the remainder $R(f, I_h)$, are used to emphasize the dependence on integrand f, and the partitioning of the interval $I_h = \{x_0 = a < x_1 < x_2 < \ldots < x_N = b\}$. For all results presented in this work the partition was uniform, which implies that $h_i = (b - a)/|I_h| \ \forall i$, therefor the bound of the error is as follows:

$$|R(f, I_h)| \leq \frac{1}{12} \|f''\|_\infty |I_h| h^3 = \frac{1}{12} \|f''\|_\infty \frac{(b-a)^3}{|I_h|^2}. \tag{4.5}$$

All fields (α, β, A, T) are sufficiently regular meaning that $\|f''\|_\infty < \infty$, therefor we can conclude that the error is of the order $\mathcal{O}(h^3)$. Since all fields were sampled using 10^4 samples, this implies that the contribution provided by the error is negligible for the leading decimals and this is sufficient for any analysis of the scaled fields $(\tilde{\alpha}, \tilde{\beta}, \tilde{A}, \tilde{T})$.

Recall that the final parameter τ, was defined using the limit,

$$\tau = \lim_{r \to \infty} T(r).$$

This limit is harder to approximate using a finite sequence. One remedy is to study the asymptotic behavior of $(\tilde{\alpha}, \tilde{\beta}, \tilde{A}, \tilde{T})$; the corresponding asymptotic expressions provide an approximation where the numerical solution intersects and follows the asymptotic expression. The fields used for this purpose are the metric fields since the inherent error for these fields are in general smaller when compared to the fermion

fields due to faster convergence. This exact methodology was employed by [5] Daniel Bakucz Canário et. al, which resulted in the following expression of the limit,

$$\tau \approx \sqrt{A(r)}T(r)\Big|_{r=r_{\max}}, \tag{4.6}$$

where A, T are elements of the unscaled solutions (α, β, A, T). This approximation of τ was also applied for all results present in this work. A rigorous bound for this error has at the time of writing, not yet been explored, but it is assumed to be small.

4.4 Solving the equations and verifying the boundary conditions

The method of choice to numerically solve non-stiff systems of ordinary differential equations is typically a Runge-Kutta method, due to their computational efficiency and simplicity. This was also the case for both Finster, Smoller and Yau [10] and Leith et. al [14]. Both groups successfully applied Wolfram's `Mathematica` language which greatly simplified the implementation of the shooting method.
To implement the shooting method in `Python`, an extension of its standard capabilities for high-precision computations is necessary. Thankfully, it is a very popular language, and thus all that is required is an external library. For this project the `Mpmath` library [17] was more than sufficient. The `Mpmath` library, is a free and comprehensive numerical library, that provides methods for various calculations using arbitrary floating-point precision, which was crucial for this project. The required decimal precision of the ω-parameter increased massively for higher values of κ and for solutions with larger central redshift z. A longer discussion about the required precision is available in Section 6.1.

The only integration method that is currently available in the `Mpmath` package is a truncated Taylor series method, the degree d of the polynomials is a parameter provided by the method. In the library this method is currently known as `odefun`. Mathematically it computes a Taylor polynomial centered at a point $r_0 \in [r_{\min}, r_{\max}]$,

$$f(r) = \sum_{n=0}^{d} \frac{\mathrm{d}^n}{\mathrm{d}s^n} f(s)\Big|_{s=r_0} (r - r_0)^n. \tag{4.7}$$

Since Taylor polynomials are local approximations, they must be moved in order to generate solutions (α, β, A, T) for the entire interval $r \in [r_{\min}, r_{\max}]$. How many intermittent r_0-points which are necessary is determined by the degree d. Furthermore, the degree also naturally effects the required computation time and accuracy. The upper bound of the accuracy of a Taylor series can be determined by its corresponding Lagrange remainder term.

Theorem 4.4.1 (Theorem 5.9 & 5.10 [19]) *Let X and Y be normed spaces. Furthermore, let W be an open subset of X. Also, if $g : W \to Y$ is n times differentiable at $\bar{x} \in W$, with $n \in \mathbb{N} \setminus \{0\}$, we define the remainder as*

$$r_n(x) := g(\bar{x} + x) - g(\bar{x}) - \sum_{k=1}^{n} \frac{1}{k!} \frac{\mathrm{d}^k}{\mathrm{d}y^k} f(y)\Big|_{y=\bar{x}} x^k.$$

Next, let $f : W \to Y$ *be* $n+1$ *times differentiable on* W *and let* $\bar{x} \in W$, $x \in X$ *be such that the segment* $[\bar{x}, \bar{x}+x]$ *is contained in* W. *If* $\left\| \frac{\mathrm{d}^{(n+1)}}{\mathrm{d}x^{(n+1)}} f(x)|_{x=w} \right\|$ *is bounded above by some* $c \in \mathbb{R}_+$ $(\mathbb{R}_+ = \{x \in \mathbb{R} : x > 0\})$ *for all* $w \in W$, *then the remainder* r_n *satisfies*

$$\|r_n(x)\| \leq \frac{c}{(n+1)!}\|x\|^{(n+1)}.$$

This theorem states that the local error for the truncated Taylor polynomial of order d (4.7), is of the order $\mathcal{O}(\|x\|^{(d+1)}/(d+1)!)$, given that the function being approximated is sufficiently smooth. Which is indeed true for the solution set (α, β, A, T), to the Einstein-Dirac equations. The accumulated error is slightly higher but is best suppressed using a sufficiently large degree d. A large degree was quite important, due to the multipeak behavior displayed by the fermion fields as we shall see shortly. But suppressing the error is not the only aspect to consider. Perform the shooting method iterations within a reasonable amount of time while ensuring accuracy of the solutions required a trade-off. Since increasing the order d also increased the required computations for all intermittent points $r_0 \in [r_{min}, r_{max}]$. The degree used to generate all results presented in this work was seven, thus the local error is of the order $\mathcal{O}(\|x\|^8/8!)$.

To discuss the verification of the relaxed boundary conditions (4.1),(4.2) we will first introduce a concept from real analysis which is useful to numerically identify convergence of sequences. A natural choice to numerically identify if a sequence a_n converges, is to employ the definition of a Cauchy sequence.

Definition 4.4.1 (Definition of a Cauchy sequence [6]) *Let* (E, d) *be a metric space. A sequence* $\{a_n\}_{n\in\mathbb{N}} \subseteq E$, *is a Cauchy sequence, if for all* $\varepsilon > 0$, $\exists N \in \mathbb{N}$ *such that*

$$d(a_n, a_m) < \varepsilon, \quad \textit{when } m, n > N. \tag{4.8}$$

An important result from functional analysis, is that all convergent sequences are Cauchy sequences. Thus, in order to identify convergence, it is sufficient to study if the numerical solutions to the fermion fields, are Cauchy sequences. To apply this definition to the Einstein-Dirac equations, which involve the fermion fields α and β, we exploit the fact that these fields should belong to a Hilbert space. Since a Hilbert space is a Banach space with a metric, induced by its inner product, we can by the completeness of Hilbert spaces identify convergent sequences of the fermion fields [6]. The fermion fields should also converge to zero for large values of r to be physically relevant, which implies that identifying convergence during the tail end of the generated sequence is sufficient. Finally, the limit of the metric field T, also follows naturally if the fermion fields converge, thus we can conclude that the shooting method implementation only needs to identify convergence of the fermion fields.

4.5 Shooting method

A well-established method to solve the Schrödinger equation $\hat{H}\psi = E\psi$, and other similar problems is the family of shooting type methods. A shooting type method is not different from "brute forcing" solutions to equations by iteratively changing the value of some parameter. But to make these methods efficient, it requires great care when selecting the updating rule for the parameter of interest. This especially applicable to problems which are sensitive to the values of the parameter, which is axiomatic property for quantum systems. For the Schrödinger equation the observable is the energy E, which is an eigenvalue of the Hamiltonian operator $\hat{H}$, acting on the eigenfunction ψ.

Applying the shooting method to the Einstein-Dirac equations involves updating the ω-parameter as part of an iteration scheme. The updating rule for the Einstein-Dirac equations had to account for if the current ω_i parameter for iterate i, was too large or small. The sets of solutions (α, β, A, T), behaved very differently based on the current parameter. For the case of ω being too small, it is identifiable by studying if $A \to 0$, which in turn caused the α and β fields to diverge. While if ω was too large, then α, β would either oscillate heavily or display oscillating behavior. There is one important remark to make at this point. Since the primary interest of this thesis was to study ground state solutions to the Einstein-Dirac equations, it was sufficient to check for zeros in the fermion fields. The presence of zeros in these fields, implies that they have crossed the r-axis, and this is a behavior which ground state solutions does not display. This behavior naturally implies that the fields are negative, which is physically not sensible. One elementary example is a vibrating string, where each harmonic is described mathematically by,

$$y_n(x) = A\sin\left(\frac{n\pi x}{L}\right), \quad x \in [0, L] \text{ and } L, A \in \mathbb{R}, \quad n \in \mathbb{N}.$$

For the first harmonic $n = 1$, the value is positive, $y_1 \geq 0$, in its given domain. This solution structure is exactly the same for the infinite square well potential in quantum mechanics [12]. In contrast to ground states, excited states—solutions ψ with higher eigenvalues E for the same Hamiltonian operator, are standing waves of higher harmonics. The number of intersections with the r-axis, depends on the level of excitation. This also holds true for the example above, where the possible excited states are described y_n for $n > 1$.

The updating rule for the ω-parameter is based on the popular binary search algorithm [21]. Its main strength is the complexity $\mathcal{O}(\log_2(N))$ [11]. The required number of operations to identify the necessary ω parameter for highly relativistic solutions, for high values of κ would be too high without an efficient search algorithm. Since in these cases, the required decimal precision was very high. The number of elements in the discretized search interval $I_\omega := [\omega_{\min}, \omega_{\max}]$ increased non-linearly based on the utilized decimal precision. In order to prove this, let $P \in \mathbb{N}$ be number of decimals used for each computation, which is parameter we can freely set in the

`Mpmath` package. Then the cardinality of the search interval set is

$$|I_\omega| = \frac{\omega_{\max} - \omega_{\min}}{10^{(-P)}} = 10^P(\omega_{\max} - \omega_{\min}) \sim \mathcal{O}(10^P).$$

Disregarding the time to perform the integration, the worst case scenario requires testing $\mathcal{O}(10^P)$ elements.

For the problem at hand, the binary search method generates an action depending on if the parameter ω is too large or small. This action narrows the next search interval based on the current parameter value. If ω is too large, then the upper bound of the search window must be updated and replaced with the current parameter. For the opposite outcome, the algorithm updates the lower bound in the search window instead. After updating the search interval, the algorithm updates ω using the midpoint of the new interval as the next parameter value.

4.6 Finding relativistic solutions

To obtain numerical solutions to the Einstein-Dirac equations corresponding to different levels of relativistic effects, such as higher or lower central redshifts (3.46), requires tuning the α_1 parameter from the initial conditions (3.38). The central redshift's dependence on α_1 is different depending on the integrator. During the initial stages of this project, the same Runge-Kutta method was also applied using the standard data-types available in the `Python` language [24]. However, it became evident quite quickly that the number of decimals, that a standard long double datatype can provide, fifteen, is insufficient to find interesting solutions to the Einstein-Dirac equations for $\kappa > 32$. To study solutions for higher numbers of particles, therefore required an extension of `Python`'s native capabilities.

For this project the library `Mpmath` was employed, and due to time constraints, it was faster and easier to use the available integration method for ODEs, instead of writing a Runge-kutta method using the library. After implementing the shooting method using the new `Mpmath` dependence, it became evident that the parameters ω, α_1 which generated the unscaled solutions (α, β, A, T), are not the same for each integration method. This implies that the central redshift value's dependence on α_1 is method dependent. But the basic principle is, higher α_1 generates higher central redshifts z. To view the relationship graphically, see Figure 4.1a. It was very time consuming to find values of α_1 for particular values of z, since the relationship between z and α_1 is exponential. Thus, for purely pragmatic reasons, I aimed to generate solutions in a small neighborhood around $z \in \{1, 7, 15, 50, 150\}$. These redshift levels was selected somewhat arbitrarily, and was necessary to compare the properties of solutions to (3.34) with different values of κ and z. However, after fixing a value for the α_1 parameter, it was not as difficult to guess the approximate value of z for $(\tilde{\alpha}, \tilde{\beta}, \tilde{A}, \tilde{T})$, based on the search interval for ω which appeared to generate (α, β, A, T). Indeed, the relationship between the unscaled ω-parameter and the resulting redshift is illustrated in Figure 4.1b. Contrary to z's dependence on α_1, $\omega(z)$ was observed to be more linear. Notice also that the order of magnitude

for the α_1 parameter might be a symptom of a small initial radius r_{min}. For $\kappa \leq 32$, the initial radius employed for all solutions soon the be presented, was $r_{\text{min}} = 10^{-5}$ which was chosen to coincide with the radius originally used by Finster, Smoller and Yau [10]. For $\kappa \geq 64$, the initial radius was increased to $r_{\text{min}} = 10^{-2}$. This decision was made in order to simplify the calculations, since the radial dependence of the initial values were of the order $r^{\kappa/2}$ for the fermion fields and r^{κ} for the metric fields (3.38). These values are completely arbitrary, and I presume that these only further differentiated the required unscaled parameters for my solutions, compared to the solutions generated by Leith et. al [14]. But the parameter which are used in any analysis are scaled and are therefore not sensitive to the various decisions made during the implementation of the shooting procedure.

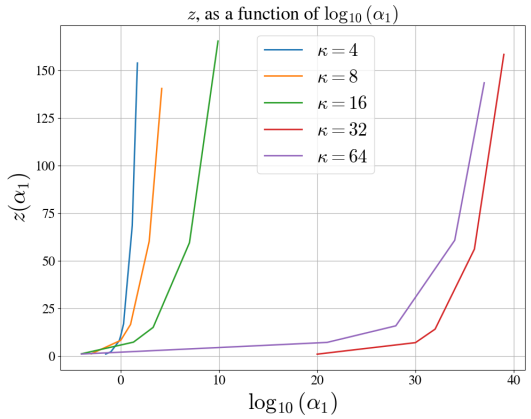

(a) The relationship between the central redshift of the scaled solutions $(\tilde{\alpha}, \tilde{\beta}, \tilde{A}, \tilde{T})$, and the unscaled initial value parameter α_1 was highly nonlinear.

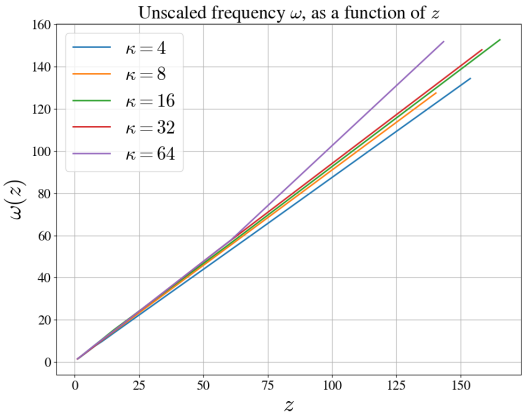

(b) The relationship between the unscaled frequency ω which generated the solutions (α, β, A, T), and the central redshift of $(\tilde{\alpha}, \tilde{\beta}, \tilde{A}, \tilde{T})$, was linear.

Figure 4.1: Two figures illustrating the relationship between model parameters and solution properties.

4.7 Summarising the shooting method algorithm

Before summarising all steps in the shooting method, we will make some final remarks. Since it is a search algorithm an initial requirement, is naturally a search interval for ω which is denoted below by I_ω. To identify a search interval required studying if the area displayed signs that a solution exists within it. The criteria which was employed in this work was to identify a ω_{min} such that the fermion fields diverged, while ω_{max} was found by studying if the same fields were in their initial stages of oscillation, since increasing ω too much caused strong oscillations with a very low amplitude. Typically, the initial stages of oscillations could be identified if either α or β was negative, which required them to cross the r-axis. Furthermore, for all solutions presented in this thesis, the parameters m and T_0 were initialized

as one, but their true physical values were later set by the scaling procedure. In the algorithm presented below, Algorithm 1, the notation $\boldsymbol{S}'(r) = \boldsymbol{f}(\boldsymbol{S}, r)$ is shorthand for (3.34). The vector $\boldsymbol{S} := [\alpha, \beta, A, T]^\top$ is a state vector while $\boldsymbol{f}$, is the collective right hand sides of the equations written as a vector. The final step after the solution set (α, β, A, T), has been identified is to scale the solutions as outlined above which finally generates the physically relevant solutions $(\tilde{\alpha}, \tilde{\beta}, \tilde{A}, \tilde{T})$.

Performing all the necessary computations while searching for sufficient ω-parameter was sometimes a lengthy procedure. This was especially the case for high values of the fermion number $\kappa > 64$ and for high levels of central redshift $z > 1$. Due to the required precision, finding $(\tilde{\alpha}, \tilde{\beta}, \tilde{A}, \tilde{T})$ for ninety particles took several hours.

Algorithm 1: Shooting method algorithm

Input: $I_\omega^{(0)} = [\omega_{\min}^{(0)}, \omega_{\max}^{(0)}]$, κ, $T_0, m, \alpha_1, r_{\min}, r_{\max}$
Output: $(\omega_f, \alpha, \beta, A, T)$

Initialise ω: $\omega^{(0)} = (\omega_{\min}^{(0)} + \omega_{\max}^{(0)})/2$
while *α & β are not normalizeable* **do**
  compute $\boldsymbol{S}(r_{\min}; \alpha_1, T_0, \kappa)$
  integrate $\boldsymbol{S}'(r) = \boldsymbol{f}(\boldsymbol{S}, r; \kappa, m, \omega^{(i)})$ for $r \in (r_{\min}, r_{\max}]$.
  if $\alpha, \beta \to 0$ **then**
    terminate
  else
    if *α or β diverges* **then**
      set $\omega_{\min}^{(i+1)} = \omega^{(i)}$
      update $\omega^{(i+1)} = (\omega_{\min}^{(i+1)} + \omega_{\max}^{(i)})/2$
      update $I_\omega^{(i+1)} = [\omega_{\min}^{(i+1)}, \omega_{\max}^{(i)}]$
    else if *$\alpha(r_i)$ or $\beta(r_i) = 0$ for $i > 0$* **then**
      set $\omega_{\max}^{(i+1)} = \omega^{(i)}$
      update $\omega^{(i+1)} = (\omega_{\min}^{(i)} + \omega_{\max}^{(i+1)})/2$
      update $I_\omega^{(i+1)} = [\omega_{\min}^{(i)}, \omega_{\max}^{(i+1)}]$

5
Results

The result section will be divided into two main sections, the first section will contain results concerning the properties of the Einstein-Dirac system. While the second section will focus on displaying results used to compare the Einstein-Vlasov system with the Einstein-Dirac system.

5.1 The structure of different solutions to the Einstein-Dirac system

The structure displayed by the fermion and metric fields from the Einstein-Dirac equation $(\tilde{\alpha}, \tilde{\beta}, \tilde{A}, \tilde{T})$, was dependent on the fermion number κ and the central redshift z. To keep the analysis brief, I will manly discuss the general traits observed for more than fifty different solutions to the Einstein-Dirac equations with different values of κ and z. The first kind of solution we will discuss, will henceforth be referred to as the canonical solution, since this solution structure did not change while increasing the fermion number. To generate the canonical solution required that the level of central redshift lied somewhere in or close to the interval [1,2], how close depends on the current number of fermions. For very few fermions, that is $\kappa \leq 4$, all redshift levels had a canonical structure. After $\kappa = 8$, larger differences were displayed, but for higher fermion numbers the canonical interval was very similar. An illustration of these solutions can be found in Figure 5.1. We will now discuss some of the canonical solutions $(\tilde{\alpha}, \tilde{\beta}, \tilde{A}, \tilde{T})$ properties. One property is the difference in amplitude between the α and β fields. To be more precise $\alpha(r) \geq \beta(r)$, the difference in amplitude is a phenomenon inherent to all solutions of the Einstein-Dirac equations. But as we soon shall discuss, there are regions where this inequality does not hold, and this will have some consequences. Contrary to the fermion fields, the metric fields displayed different types of behavior. First, we will discuss the radial metric field $A(r)$. Initially, it appears to be almost constant and beyond this point the field would decrease until a global minimum was reached, past this point the field would start to increase and converge to one, in accordance with the asymptotic flatness requirement. Next, the metric's time component field $T(r)$. Similarly, to A, the field also appears to be almost constant for a small neighborhood to $r = 0$. Beyond this region the field is decreasing monotonically, and asymptotically approach the asymptotic flatness limit $T(r) \to 1$ as $r \to \infty$.
To find solutions where the structure was substantially different from the canonical structure required larger central redshifts. The emergent structure is henceforth dependent on the number of fermions in the system. For a sufficiently small $\kappa \leq 32$,

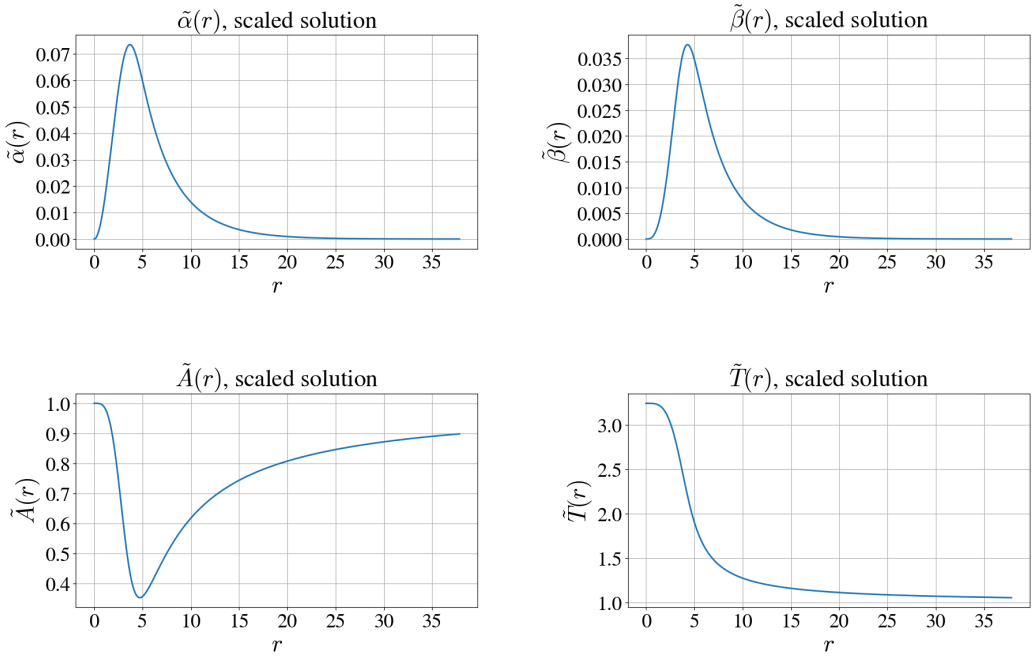

Figure 5.1: The canonical structure of all fields $(\tilde{\alpha}, \tilde{\beta}, \tilde{A}, \tilde{T})$ when $z \sim 1$, from the Einstein-Dirac equation.

increasing the redshift, resulted in less cohesive fermion fields. The fields were less cohesive in the sense that small regions containing extra peaks started to appear in the canonical structure of the fermion fields. We will refer to this property as a multipeak behavior, following the naming convention used by Andréasson and Rein [3]. To view an example, see Figure 5.2. The occurrence of the additional peaks in the fermion fields was also reflected in the metric fields. Starting with the radial metric field A, this field has an increased amount of local extremum points compared to Figure 5.1. Furthermore, these extra peaks arise in this field at a similar radius to the fermion fields. In contrast to the radial metric field, the time component of the metric has undergone more subtle changes. Instead of displaying more peaks in the plot, there are instead a few radial distances where the T field, undergoes changes in the magnitude of its derivative. However, its monotonically decreasing behavior remained unchanged.

In order to find solutions where the peaks from the fermion fields are more separated, required a sufficiently high κ while tuning the redshift z. Leith et. al [14] called these solutions, gravitationally self-trapped solutions, the structure of the fermion fields are in this case very different to the canonical solution we discussed previously. An example of gravitationally self-trapped solution is described by the parameter pair $\kappa = 90$ and $z \approx 7.7$, to view a plot of the corresponding solution set $(\tilde{\alpha}, \tilde{\beta}, \tilde{A}, \tilde{T})$, see Figure 5.3. The fermion fields are noticeably different to the previous case, but the metric fields still display the same behavior.

We will finish the discussion about the structure of the solutions by considering solutions with very high central redshift. These solutions, akin to solutions with $z \approx 1$, were very similar, independent of the current κ parameter. By using $\kappa = 90$

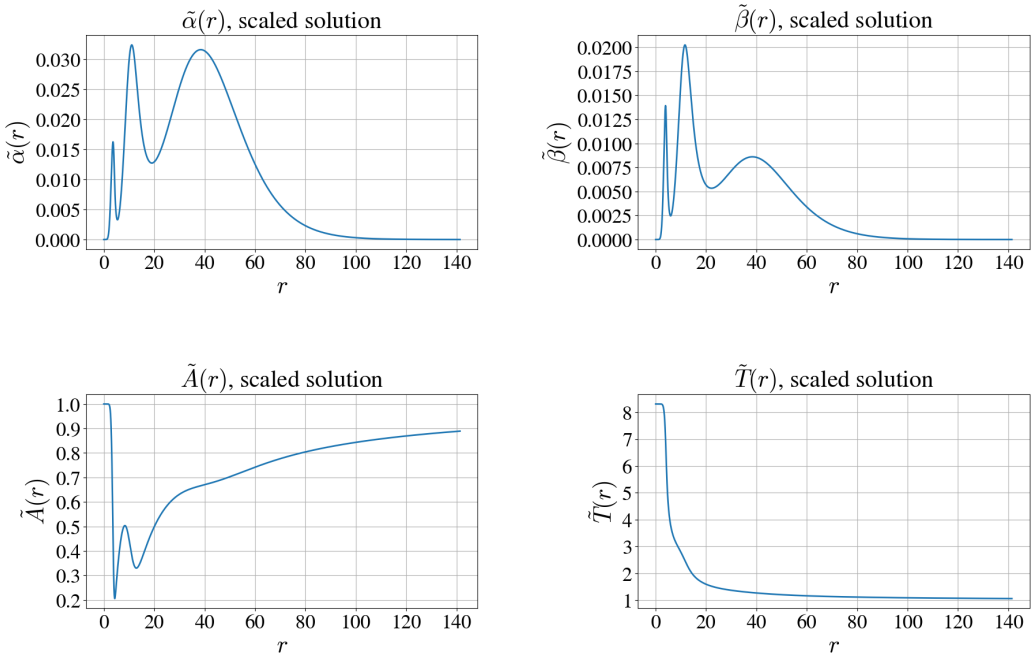

Figure 5.2: Extra peaks start to emerge in the canonical solutions $(\tilde{\alpha}, \tilde{\beta}, \tilde{A}, \tilde{T})$ in Figure 5.1, when the level of central redshift z, increased.

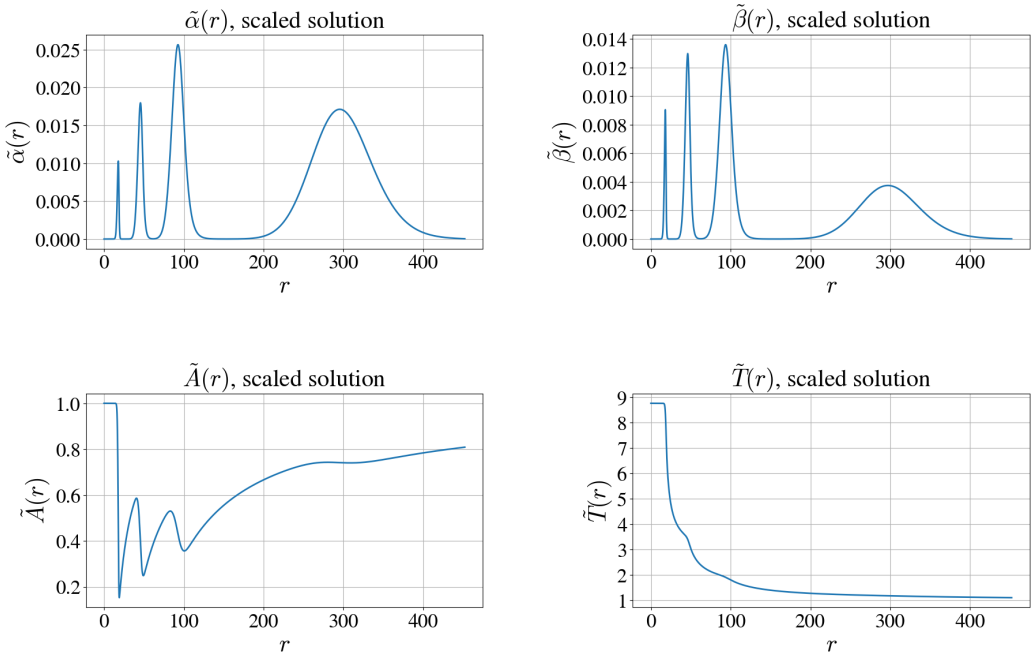

Figure 5.3: When κ is high enough and the redshift is sufficiently tuned, the resulting fermion fields are more separated than when the peaks starts to emerge, compare this with the case when the peaks start to appear in Figure 5.2.

as before and increasing z to approximately $z \approx 148.6$. The resulting solution is visually similar to the case when the extra peaks started to emerge, see Figure

5.4. What differentiates the two cases are mainly that the number of peaks in the multipeak configuration are very high. Furthermore, the behavior of the metric fields is similar, but more extreme due to the large amount peaks present in the fermion fields. In particular, the structure of metric's time component is very similar to an inverted Heaviside step function. Which physically implies a strong and very local time distortion. Finally, the radial component of the metric oscillates very heavily due to the high number of peaks.

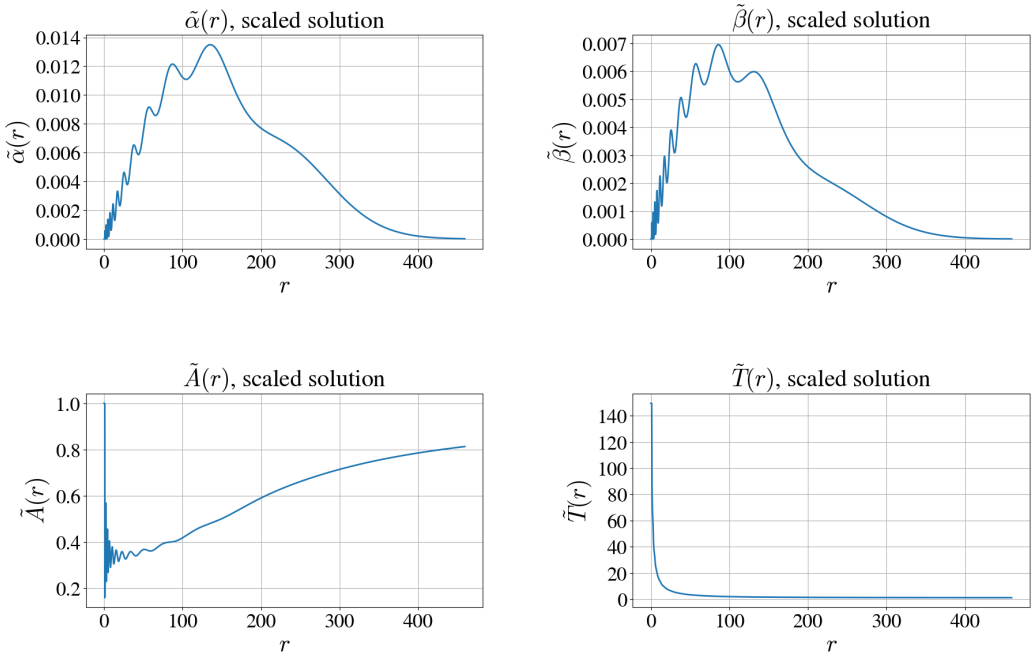

Figure 5.4: For solutions with very high levels of central redshift, the resulting structure is very similar to the case when the peaks start to emerge, compare the fermion fields with Figure 5.2.

5.2 Einstein-Dirac system properties

All presented results in this section concern the different matter properties defined in Section 3.8 for some solutions to the Einstein-Dirac equations. First, we will discuss the radial pressure, after discussing the radial pressure I will show some results from studying the following inequality $p_r + 2p_\perp \leq \Omega \cdot \rho$. Finally, after the inequality has been investigated, we finish by studying the compactness property for many solutions.

5.2.1 Properties of the radial pressure

While studying the emergent matter properties for the Einstein-Dirac equations, I identified regions with negative radial pressure p_r, to view an example see Figure 5.5. These regions became narrower as the central redshift z increased. Negative pres-

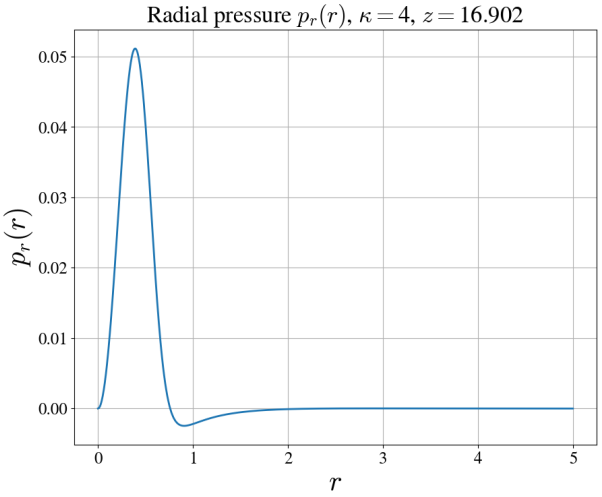

Figure 5.5: The radial pressure p_r for a particular solution the Einstein-Dirac equation. Note that there is a small region where the pressure is negative.

sure, is a property presumed to be displayed by exotic matter, such as dark energy [13]. The disappearance of these regions can thus be used to identify a transition of the quantum fields inherent quantum mechanical behavior into more classical behavior. Indeed, by plotting the minimal value of the observed radial pressure function, for different values of κ and different levels of z, we obtain evidence for a transition to more classical matter behavior, see Figure 5.6. The figure displays only a selection of states where $\kappa \in \{2, 4, 8, 16\}$, since these regions disappear completely for solutions with $\kappa > 16$. We can also see that regions with negative pressure only emerge while studying relativistic states, as the canonical solutions (Figure 5.1) does not have any regions with negative pressure. This implies that regions with negative pressure are an emergent property from the relativistic effects displayed by the solutions $(\tilde{\alpha}, \tilde{\beta}, \tilde{A}, \tilde{T})$, when the number of fermions was sufficiently small.

5.2.2 Properties of the matter pressures and the energy density

As we discussed in Section 3.5, we require that the Einstein-Dirac system must fulfil some assumptions so that Andreasson's theorem [1] can guarantee a upper bound for the compactness of static spherical symmetric solutions to Einstein's field equations (3.8),

$$\Gamma := \sup_{r>0} \frac{2m(r)}{r}.$$

In the previous section we found requirements to ensure a positive radial pressure, next we will consider the following inequality,

$$p_r + 2p_\perp \leq \Omega \cdot \rho.$$

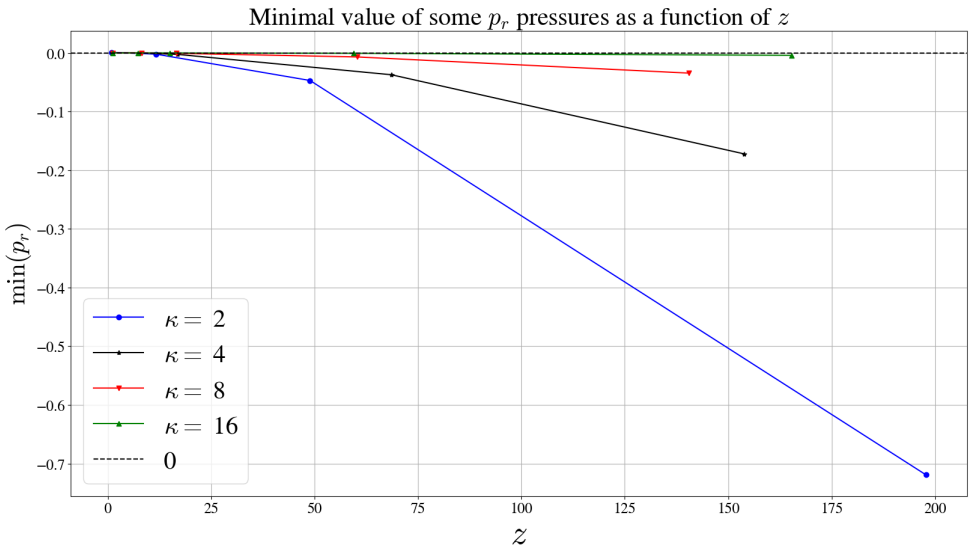

Figure 5.6: The minimal values of the radial pressure p_r for a selection of solutions the Einstein-Dirac equation. Quite counter-intuitively, these regions disappeared for solutions where $\kappa \geq 16$.

For purely numerical purposes, it is easier to study the inequality using a fraction,

$$\frac{p_r + 2p_\perp}{\rho} \leq \Omega. \tag{5.1}$$

If this fraction becomes larger than one, then this an indicator that Ω is bigger than one, which implies that the compactness bound for Vlasov, namely 8/9 [3], might not hold for the Einstein-Dirac system. To be more precise, I would like to identify the supremum of the parameter such that the inequality holds,

$$\sup_{\Omega>0} \frac{p_r + 2p_\perp}{\rho} \leq \Omega.$$

But this is no easy task, and the results indicate that the supremum of Ω appears to be dependent on both κ and the relativistic nature of the solutions. In particular, multipeak configurations with more separated peaks are particularly interesting since this structure displayed greater values of the fraction (5.1) than the other structures discussed in Section 5.1. In order to summarize my findings, I plotted the maximum value of the fraction

$$\max_{r\in[r_{\min},r_{\max}]} \left\{ \frac{p_r(r) + 2p_\perp(r)}{\rho(r)} \right\},$$

for different levels of central redshift and different number of fermions. See Figure 5.7 for the resulting plot. By studying the radius where the compactness attains it largest value, I found that the quotient was smaller and for these radii the quotient was quite close to one. Before displaying these results, we will define the radius r_*

$$r_* := \arg\max_{r\in[r_{\min},r_{\max}]} \left\{ \frac{2m(r)}{r} \right\}. \tag{5.2}$$

Based on the results in Figure 5.7, it is clear that Ω appears to be one, for non-canonical solutions, and for $\kappa \geq 8$, hence Figure 5.8 displays results for $p_r(r_*) + 2p_\perp(r_*)/\rho(r_*)$, excluding the canonical solutions.

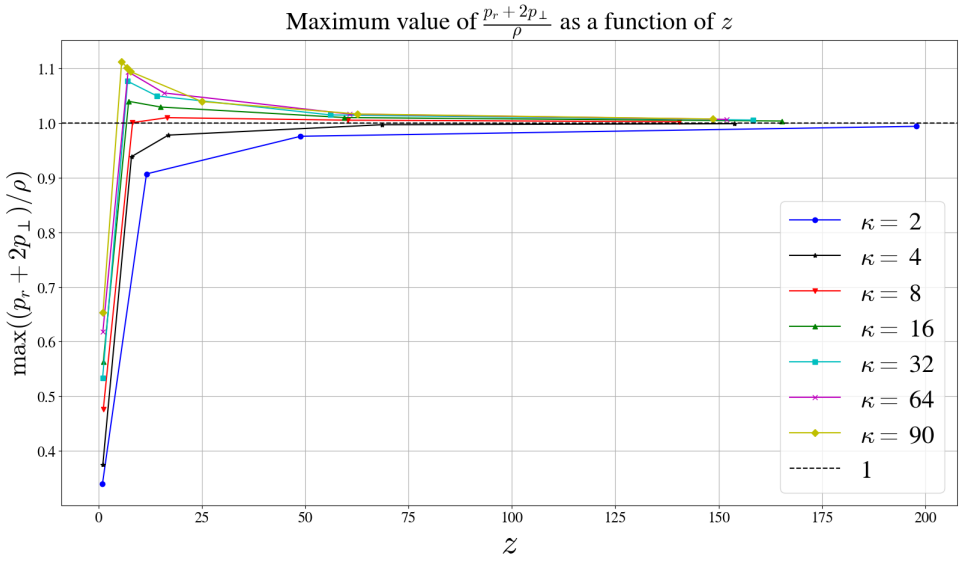

Figure 5.7: The maximal value of the inequality fraction (5.1), as a function of central redshift's value z, for some κ values.

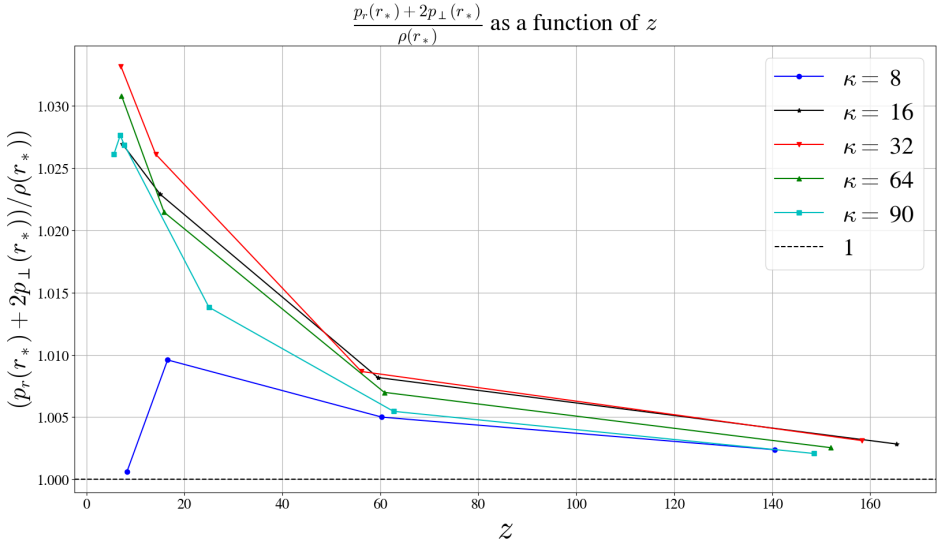

Figure 5.8: The value of the inequality fraction (5.1), sampled at the radius where Γ (3.11) attains its largest value (5.2), as a function of central redshift z, for fermion numbers $\kappa \in [8, 16, 32, 64, 90]$.

5.2.3 Compactness results for the Einstein-Dirac system

Since we have investigated the sign of the radial pressure and the energy density/ pressure inequality, what remains is to investigate the values of the compactness

itself. The compactness $2m(r)/r$, was defined using the Schwarzschild metric and its largest value is a signature inherent to all solutions to Einstein's field equations. The largest compactness value,

$$\max_{r\in[r_{\min},r_{\max}]}\left\{\frac{2m(r)}{r}\right\} \overset{(5.2)}{=} \frac{2m(r_*)}{r_*}, \tag{5.3}$$

increased while increasing κ, it was also observed that, higher levels of central redshift beyond the canonical solution, did not strongly affect the compactness of the system. Similarly to the previous figure, I plotted the largest compactness value against the central redshift, for the same solutions presented in Figure 5.7. The resulting plot is available in Figure 5.9.

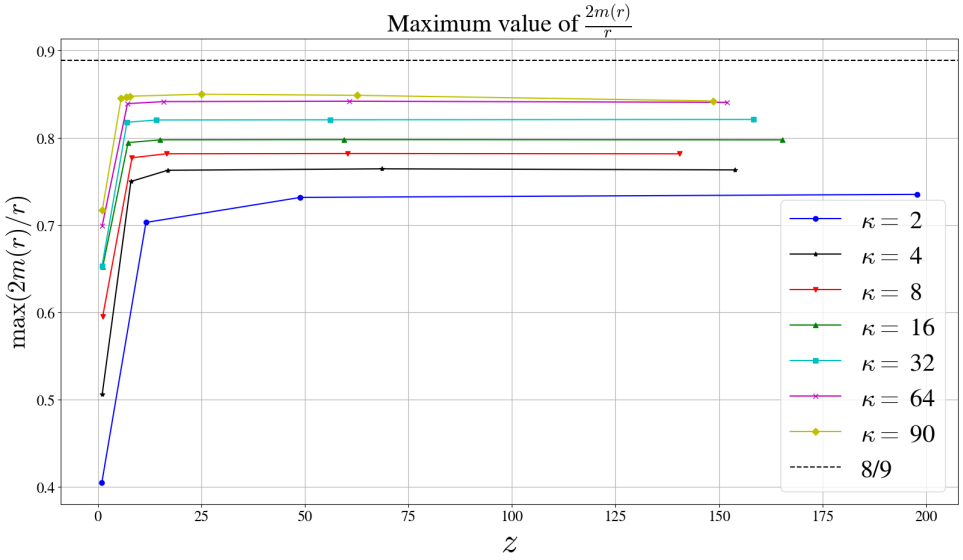

Figure 5.9: Largest compactness values associated with the solutions from the inequality results in Figure 5.7.

5.3 Comparing energy density functions for the Einstein-Dirac and Einstein-Vlasov system

The final set of results in this report concern comparing the distribution of matter in both the Einstein-Dirac system and the Einstein-Vlasov system, where the latter is introduced in Section 3.10. In [3] Andréasson and Rein, scaled the energy density function ρ, which we introduced in Definition 3.8.1 and Definition 3.10.1 for the Einstein-Dirac system and the Einstein-Vlasov system, respectively. The reason for scaling ρ was to display the succeeding peaks more clearly after the first and dominant peak, since the amplitude of the first peak was large in comparison to the others. We will define the scaled energy density below,

$$\tilde{\rho}(r) = \log\Big(4\pi r^2\rho(r) + 1\Big). \tag{5.4}$$

In the case of the Einstein-Dirac system we must first solve its differential equations and then use the set of scaled fields $(\tilde{\alpha}, \tilde{\beta}, \tilde{A}, \tilde{T})$ to define ρ, while the Einstein-Vlasov system requires numerical methods to approximate the required integrals. In this section we will study two very similar energy density functions for both the Einstein-Dirac and Einstein-Vlasov system. This comparison is not quantitative and is purely visual. To simplify the visual comparison, each sample point $(r_i, \tilde{\rho})$ is plotted assuming $r_i := t$, where t is similar to a curve parameter $\gamma(t) = [x(t), y(t)]^\top$, and thus $t \in [0, 1]$. Furthermore, the amplitudes are normalized with respect to the amplitude of the dominant peak. It also necessary to add a comment, that the energy densities presented below are not the only cases where the two systems produce similar matter distributions, in fact, similar distributions were very common. The first energy density distribution is constructed using the $\kappa = 16$ and $z = 7.3101$ state, while the Vlasov distribution was constructed using the parameter set $(k = 0, l = 7, L_0 = 0, y_0 = 0.118)$; both are illustrated in Figure 5.10. The final result we will consider is the energy density for the Einstein-Dirac solution when $\kappa = 90$ and $z = 25.0165$, the corresponding parameter set for the Einstein-Vlasov system was $(k = 4.5, l = 19.5, L_0 = 2.3, y_0 = 0.0398)$, see Figure 5.11 for the resulting plots. A final comment, is that it is possible to generate scaled energy densities with greater similarities, but this would require a parameter identification method for Vlasov's polytropic ansatz parameters k, l, L_0, y_0 (3.51), and due to time constraints, unfortunately had to be omitted. Each result is nevertheless visually similar. The discrepancies in the amplitudes and local curvature differences are also reflected in the computed redshifts for the Vlasov and Dirac systems. Indeed, for the first density the computed central redshift for the Vlasov system was $z = 8.578628$, for the second density the central redshift was $z = 25.981807$ for the Vlasov system. Finally, the maximum compactness of both solutions is also quite close, in particular the first comparison is visually alike, while the difference in central redshift and maximum compactness are smaller compared to the second example.

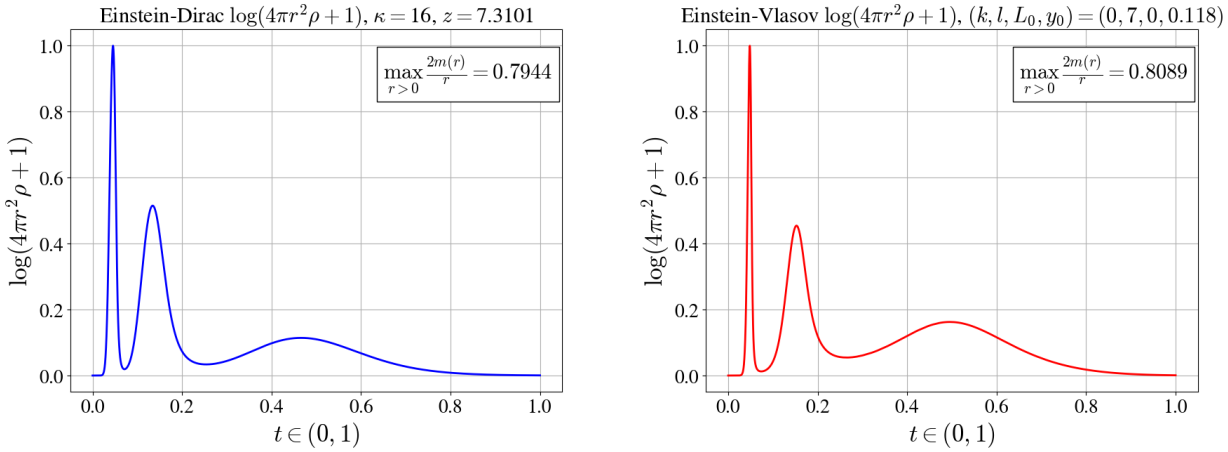

Figure 5.10: The figure displays plots of the scaled energy density $\log(4\pi r^2\rho+1)$, for the Einstein-Dirac system to the left (blue) and the Einstein-Vlasov system to the right (red). Note that they are strikingly similar and notice that their respective maximum compactness is also similar in magnitude.

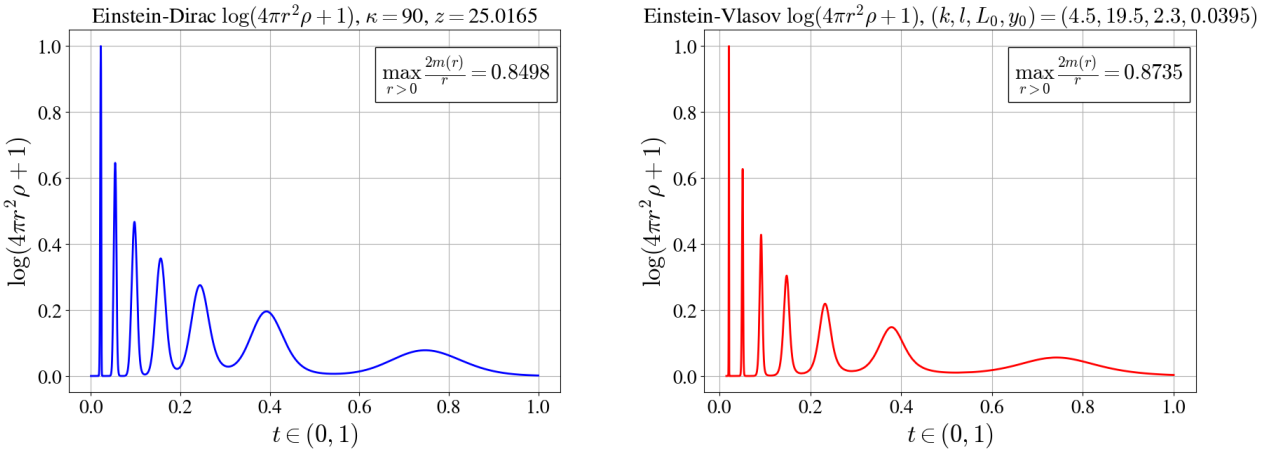

Figure 5.11: The figure displays plots of the scaled energy density $\log(4\pi r^2\rho+1)$, for the Einstein-Dirac system to the left (blue) and the Einstein-Vlasov system to the right (red). Note that they are strikingly similar and notice that their respective maximum compactness is also similar in magnitude.

6

Discussion and conclusions

6.1 A discussion on the required numerical precision

Before discussing any results and their implications, we will dedicate this section to comment on one complication for the computations performed during the shooting method. In order to identify normalisable fermion fields and properly behaved metric fields, we must identify "the correct" eigenvalue parameter ω from the Einstein-Dirac equations (3.30). The parameter is introduced into the equations by the plane wave ansatz (3.29), and is by definition an eigenvalue to the Hamiltonian operator $\hat{H}\Psi = \omega\Psi$. Due to fact that the parameter is an eigenvalue, we cannot freely set this parameter and expect a physically sensible solutions to the Einstein-Dirac equations. The inherent difficulty due to the required parameter identification is also present for a simpler case where the Dirac equation is not coupled to the gravitational description, in [22] Goldman and Silbar discuss the same problem in the context of the Radial Dirac equation for a few different potentials.

Attacking this problem numerically is therefor difficult, as there is theoretically only one parameter ω which yields a proper solution for a fixed κ and α_1 (related to the central redshift z). The main numerical difficulties this provides is the identification of a ω parameter to the unscaled problem "that is good enough". To be more precise, if ω is not provided to a sufficient level of accuracy, this causes the numerical solutions of the fermion fields to diverge, where the field diverges is dependent on current number of "correctly identified" decimals for ω. If the correct amount of decimals is too few, for $r < r_{\max}$, then the fields will diverge up until a sufficient accuracy is reached, and the required precision will only increase if a larger $r_{\max}$ is required to capture the behavior of all fields (α, β, A, T). The required level of precision for solutions to the Einstein-Dirac system increased substantially, for configurations with many particles, in particular for $\kappa = 90$, the level of precision I used in my calculations were around 80 decimals. After fixing κ, searching for solutions with higher central redshifts z, revealed that the sensitivity of the solution with respect to ω, increased. The high required precision, necessitated the application of a fast and efficient search algorithm, for this task the Binary search algorithm was a natural choice, due to the fact that the discretized search interval $[\omega_{\min}, \omega_{\max}]$ is by construction an ordered list, which is an requirement to apply it as a updating rule in the parameter identification procedure.

6.2 Einstein-Dirac solution structure

The identified solution types were based exclusively on my recorded solutions, and a greater sample size might be necessary to make more conclusions about the structure of all fields $(\tilde{\alpha}, \tilde{\beta}, \tilde{A}, \tilde{T})$, but the observation: larger central redshift z, yields more peaks is true and can thus safely be proclaimed. The canonical solutions distinguished itself from the other configurations, due to their non-relativistic nature but requires more analytical work to study the reason why. Also, the moderately relativistic solutions, meaning $z \in [5, 10]$, were particularly interesting, both when considering the largest ratio (5.1) and the ratio when the compactness (3.11) achieved its maximum; since the relativistic regime differences implies both a z and κ (particle number) dependence for Ω in (3.14), based on Figure 5.7 and Figure 5.8. The results displayed by both figures are different, and the amplitudes of the inequality fraction is subject to greater scepticism than those displayed in the second figure. This is because the maximal value of

$$\frac{p_r + 2p_\perp}{\rho},$$

tended to occur in the tails between the initial peaks, where the amplitudes of the fermions fields were very small, and of the order $\alpha, \beta \sim 10^{-8}$. In contrast to this we can be more certain about the amplitudes in second figure, since the inequality fraction at r_*,

$$\frac{p_r(r_*) + 2p_\perp(r_*)}{\rho(r_*)}, \quad r_* = \underset{r\in[r_{\min}, r_{\max}]}{\arg\max} \left\{ \frac{2m(r)}{r} \right\},$$

was defined with fields with much larger amplitude, see for example the fermion fields in Figure 6.1. This adds an extra level of complexity to investigation the compactness. But it would be more natural to associate the $\Omega \cdot \rho$ bound with the radius at which the compactness is largest. However, the conclusion that $\Omega > 1$ and that Ω is dependent on both κ and z is strengthened by both results. Given more time, it would preferable to perform the computations associated with Figure 5.7 with Taylor polynomials of higher degree (see section 4.4), but I strongly suspect that it will not impact this conclusion.

6.3 Negative radial pressure

The existence of regions with negative matter pressures is atypical for classical matter models, and furthermore, the fact that negative radial pressure regions disappear for $\kappa \geq 16$ was highly unexpected, see Figure 5.6. From a physical point of view this was highly unexpected, since quantum effects typically vanish only when studying very large ensembles of particles. Based on this result, we have evidence for a transition to more classical matter behavior from the quantum fields α, β derived from the Dirac equation. This result should motivate further studies into the emergence of classical properties from the quantum fields, inherent to the Einstein-Dirac system.

6.4 Pressure and density inequality results

Before discussing the numerical results it is insightful to first study the inequality fraction (5.1) analytically, to do so the definition in Section 3.8 is necessary. Using the definitions for the pressures and energy density we can write the fraction as

$$\frac{p_r(r) + 2p_\perp(r)}{\rho(r)} = \frac{\omega T(r)(\alpha^2(r) + \beta^2(r)) - m(\alpha^2(r) - \beta^2(r))}{\omega T(r)(\alpha^2(r) + \beta^2(r))}.$$

Hence, if the inequality is greater than one, we get a condition for the fermion fields,

$$\frac{\omega T(r)(\alpha^2(r) + \beta^2(r)) - m(\alpha^2(r) - \beta^2(r))}{\omega T(r)(\alpha^2(r) + \beta^2(r))} \geq 1 \Rightarrow \boxed{\beta(r) \geq \alpha(r)}. \tag{6.1}$$

Thus, if the inequality parameter $\Omega > 1$, then this implies that $\beta(r)$ is greater than $\alpha(r)$. The numerical results displays evidence that the bounding factor Ω is greater than one for non-canonical solutions when $\kappa \geq 8$, see Figure 5.7 and 5.8. As a matter of fact, all results where the (5.1) fraction is greater than one, the analytical result (6.1) holds true. Indeed, to display this we will consider one case, namely $\kappa = 90$ and $z = 6.8977$, to view a figure displaying the fermion fields α,β and the inequality fraction at the radius (5.2), see Figure 6.1. By studying the fermion fields it is clear that compactness attains its largest value while $\alpha(r) < \beta(r)$, which is rarely the case, see for example Figure 5.1 - Figure 5.4. Alongside the numerical results, the known theory about the Dirac equation, in particular the results describing the amplitude of the Spinor's components as was discussed in Section 3.6.2, tells us that locally the fermion fields can be dominated by the anti-particle component. In for example [23] chapter 1, Thaller describes that general solutions for Dirac's equation for a free particle, is a linear combination of the positive and negative energy Spinors. In the case of the Einstein-Dirac system the anti-particle component is described by β, and we can also conclude from Figure 5.7, that highly relativistic solutions (high z) are not locally dominated by the β-field to the same degree, and the fraction should converge to one for $z \to \infty$. It also worth to noting that the difference in amplitude between α and β became less pronounced while increasing z, in particular, for low radii, since the α-field tended to dominate the other β-field after a certain radius was reached. Furthermore, due to the results in Section 5.2.3, in particular Figure 5.9, illustrates evidence that the compactness of the solutions $(\tilde{\alpha}, \tilde{\beta}, \tilde{A}, \tilde{T})$, are not 8/9 which would follow from $\Omega = 1$. Hence, based on the numerical results and the general theory about the Dirac equation, we have strong evidence that for some configurations, the bounding parameter is greater than one, $\Omega > 1$, which stands in contrast to the 8/9 compactness bound for the Einstein-Vlasov system [3]. Furthermore, the compactness as implied by inequality ratio results, for non-canonical solutions is dependent on κ and ω, which follows from the results in Figure 5.9.

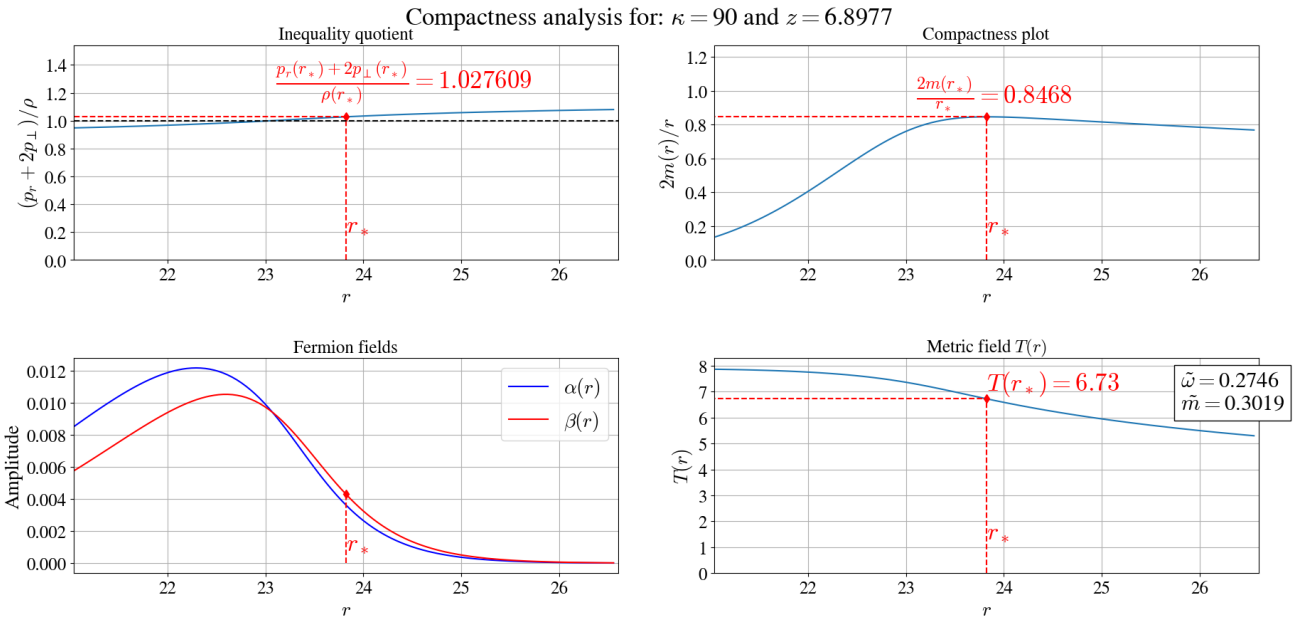

Figure 6.1: This figures contains four subplots, the first subfigure displays the inequality fraction when the compactness in the second figure attains its largest value. Similarly, the final row displays the fermion fields and highlights $\beta(r_*) > \alpha(r_*)$ (left), and the metric field $T(r_*)$ (right), along with the scaled mass and frequency $\tilde{m}$ and $\tilde{\omega}$.

6.5 Comparing the Einstein-Vlasov and the Einstein-Dirac system

This comparison is interesting based on two perspectives, first and foremost, the main motivation for this project was that the solutions presented in Leith et. al's paper [14] appeared to have similar features to the distributions generated by the Vlasov system. Secondly, based on the encountered quantum to classical transition, this would imply that the Einstein-Vlasov system and the Einstein-Dirac system would constitute a compelling pairing to dwell deeper and study under what conditions a quantum system becomes more classical. This final point appears to be true since it is possible to generate very similar matter distributions as was outlined in Section 5.3. This can also be motivated heuristically with a physical argument; at least one parameter available in the polytropic ansatz for the Einstein-Vlasov system (3.51) is related to the angular momenta in the system, and by construction κ is also related to the total angular momentum $\kappa = 2j + 1$, see Section 3.7. Thus, I strongly suspect that it should be possible to show a more rigorous correspondence between the fermion number and the angular momentum parameter. We can also connect the available momentum to the Dirac system's quantum properties, since we established that the threshold to classical behavior can be found by studying the number of fermions in the system. This connection should also motivate further studies into the two systems where the Vlasov system is a possible candidate for a

classical limit of the Einstein-Dirac system. Beyond the established visual similarities, we are also able to add another comment that both the central redshift and the maximum compactness were alike in both presented comparisons. I should also add that the difference in their respective numerical values is most likely caused by the slight discrepancies in amplitude and local curvature between the densities produced by the Einstein-Dirac and Vlasov systems, and it would therefore be interesting to use a more sophisticated parameter identification procedure for the Vlasov parameters, and afterwards, yet again, compare both the compactness and central redshift.

6.6 Final remarks

The results of this work indicate that the Einstein-Vlasov and the Einstein-Dirac system might constitute an intriguing pairing for future studies of transitions of quantum to classical matter properties. There are many ways to expand the scope of this study, one aspect that would be interesting to study is whether excited states display similar properties to the ground state discussed in this work. During the initial stages of this project a restriction to study ground state configurations was made, the first reason was the universe's tendency to naturally prefer low energy configurations, on the other hand, excited states were also more difficult to identify due to the presence of degeneracy in the excited states [14],[5]. Another goal is to perform a similar study of the Einstein-Dirac-Maxwell system [9], which in contrast to the Einstein-Dirac system introduces charge to all particles within the single shell configuration, which we suspect would increase the compactness displayed by the system. Finally, due to the nature of this work, a larger sample size of solutions would be useful, in particular while studying the compactness of the moderately relativistic solutions $z \in [5, 10]$, as these configurations displayed strong evidence that $\Omega > 1$, from the matter pressure and energy density inequality.

To summarize all results in this thesis, by numerical investigations we have found that the compactness bound for the Einstein-Dirac system is different for some configurations when compared to the bound for the Vlasov system, $2m(r)/r \leq 8/9$, which was caused by the anti-particle spinor component from the Dirac equation. But even though that this was the case, both systems are remarkably similar. The list of similarities are as follows, a similar multipeak or multimodal behavior in the energy density functions, and even though the anti-particle could locally dominate the other field, in these regions the required Ω-parameter introduced in Section 5.2.3, is still very close to one. Finally, while studying the properties of the Einstein-Dirac system, we were also able to find evidence for type of quantum to classical matter behavior transition. Contradictory to the general intuition that classical behavior requires millions of particles, the Einstein-Dirac system appears to transition at only a handful of particles; that is $\kappa \geq 16$.

Bibliography

[1] H. Andréasson, "Sharp bounds on 2m/r of general spherically symmetric static objects," *Journal of Differential Equations*, vol. 245, no. 8, pp. 2243–2266, Oct. 2008. DOI: 10.1016/j.jde.2008.05.010.

[2] H. Andréasson, "The einstein-vlasov system/kinetic theory," *Living Reviews in Relativity*, vol. 14, no. 1, May 2011. DOI: 10.12942/lrr-2011-4.

[3] H. Andréasson and G. Rein, "On the steady states of the spherically symmetric einstein–vlasov system," *Classical and Quantum Gravity*, vol. 24, no. 7, p. 1809, Apr. 2007. DOI: 10.1088/0264-9381/24/7/008.

[4] H. A. Buchdahl, "General relativistic fluid spheres," *Phys. Rev.*, vol. 116, pp. 1027–1034, 4 Nov. 1959. DOI: 10.1103/PhysRev.116.1027.

[5] D. B. Canário, S. Lloyd, K. Horne, and C. A. Hooley, "Infinite-redshift localized states of dirac fermions under einsteinian gravity," *Physical Review D*, vol. 102, no. 8, Oct. 2020. DOI: 10.1103/physrevd.102.084049.

[6] L. Debnath and P. Mikusinski, *Introduction to Hilbert Spaces with Applications*. Elsevier Science, 2005, ISBN: 9780122084386.

[7] S. Dragomir, P. Cerone, and A. Sofo, "Some remarks on the trapezoid rule in numerical integration," *Indian Journal of Pure & Applied Mathematics*, vol. 31, May 2000.

[8] F. Finster, J. Smoller, and S.-T. Yau, "Non-existence of black hole solutions¶for a spherically symmetric, static einstein-dirac-maxwell system," *Communications in Mathematical Physics*, vol. 205, no. 2, pp. 249–262, Aug. 1999. DOI: 10.1007/s002200050675.

[9] F. Finster, J. Smoller, and S.-T. Yau, "Particle-like solutions of the einstein–dirac–maxwell equations," *Physics Letters A*, vol. 259, no. 6, pp. 431–436, Aug. 1999. DOI: 10.1016/s0375-9601(99)00457-0.

[10] F. Finster, J. Smoller, and S.-T. Yau, "Particlelike solutions of the einstein-dirac equations," *Physical Review D*, vol. 59, no. 10, Apr. 1999. DOI: 10.1103/physrevd.59.104020.

[11] I. Flores and G. Madpis, "Average binary search length for dense ordered lists," *Commun. ACM*, vol. 14, no. 9, pp. 602–603, Sep. 1971, ISSN: 0001-0782. DOI: 10.1145/362663.362752.

[12] D. J. Griffiths and D. F. Schroeter, *Introduction to quantum mechanics*. Cambridge University Press, 2018, ISBN: 1107189632.

[13] S.-W. Kim, "The physical properties of exotic matter," *Journal of The Korean Physical Society - J KOREAN PHYS SOC*, vol. 54, Jun. 2009. DOI: 10.3938/jkps.54.2196.

[14] P. E. Leith, C. A. Hooley, K. Horne, and D. G. Dritschel, "Fermion self-trapping in the optical geometry of einstein-dirac solitons," *Physical Review D*, vol. 101, no. 10, May 2020. DOI: 10.1103/physrevd.101.106012.

[15] H. Maeda and T. Harada, "Criteria for energy conditions," *Classical and Quantum Gravity*, vol. 39, no. 19, p. 195 002, Aug. 2022. DOI: 10.1088/1361-6382/ac8861.

[16] L. Maiani and O. Benhar, *Relativistic quantum mechanics : an introduction to relativistic quantum fields.* CRC Press, 2015, ISBN: 9781498722308.

[17] T. mpmath development team, *Mpmath: A Python library for arbitrary-precision floating-point arithmetic (version 1.3.0)*, http://mpmath.org/, 2023.

[18] B. O'Neill, *Semi-Riemannian geometry : with applications to relativity.* (Pure and applied mathematics: 103). Academic Press, 2008, ISBN: 0125267401.

[19] J.-P. Penot, *Analysis: From Concepts to Applications.* (Universitext). Springer International Publishing, 2016, ISBN: 9783319324111.

[20] J. J. Sakurai and J. Napolitano, *Modern Quantum Mechanics.* Cambridge University Press, 2021, ISBN: 9781108473224.

[21] R. Sedgewick and K. D. Wayne, *Algorithms.* Addison-Wesley, 2011, ISBN: 032157351X.

[22] R. R. Silbar and T. Goldman, "Solving the radial dirac equations: A numerical odyssey," *European Journal of Physics*, vol. 32, no. 1, pp. 217–233, Dec. 2010. DOI: 10.1088/0143-0807/32/1/021.

[23] B. Thaller, *The Dirac Equation* (Theoretical and Mathematical Physics). Springer Berlin Heidelberg, 2013, ISBN: 9783662027530.

[24] G. Van Rossum and F. L. Drake, *Python 3 Reference Manual*. Scotts Valley, CA: CreateSpace, 2009, ISBN: 1441412697.

[25] P. Virtanen *et al.*, "SciPy 1.0: Fundamental Algorithms for Scientific Computing in Python," *Nature Methods*, vol. 17, pp. 261–272, 2020. DOI: 10.1038/s41592-019-0686-2.

[26] R. M. Wald, *General relativity*. Chicago, IL: Chicago Univ. Press, 1984.

[27] S. Weinberg, *Gravitation and Cosmology: Principles and Applications of the General Theory of Relativity*. New York: John Wiley and Sons, 1972, ISBN: 978-0-471-92567-5.

A

Appendix 1

A.1 Scaling the metric and fermion fields

Inserting the transformed variables into the first differential equation:

$$\alpha'(r) = \frac{\kappa}{2r\sqrt{A(r)}}\alpha(r) - \frac{(\omega T(r) + m)}{\sqrt{A(r)}}\beta(r),$$

yields the following result

$$\begin{aligned}
\tilde{\alpha}'(r) &= \lambda\sqrt{\frac{\tau}{\lambda}}\alpha'(\lambda r) \\
&= \lambda\sqrt{\frac{\tau}{\lambda}}\left[\frac{\kappa}{2(\lambda r)\sqrt{\tilde{A}(r)}}\sqrt{\frac{\lambda}{\tau}}\tilde{\alpha}(r) - \frac{(\frac{\tilde{\omega}}{\lambda\tau}(\tau\tilde{T}(r)) + \frac{\tilde{m}}{\lambda})}{\sqrt{\tilde{A}(r)}}\sqrt{\frac{\lambda}{\tau}}\tilde{\beta}(r)\right] \\
&= \frac{\kappa}{2r\sqrt{\tilde{A}(r)}}\tilde{\alpha}(r) - \frac{(\tilde{\omega}\tilde{T}(r) + \tilde{m})}{\sqrt{\tilde{A}(r)}}\tilde{\beta}(r).
\end{aligned}$$

Which in the end yields an identical differential equation with the transformed variables and parameters $\omega \to \tilde{\omega}$ and $m \to \tilde{m}$.

DEPARTMENT OF SOME SUBJECT OR TECHNOLOGY
CHALMERS UNIVERSITY OF TECHNOLOGY
Gothenburg, Sweden
www.chalmers.se

CHALMERS
UNIVERSITY OF TECHNOLOGY